minerals

MDPI

Article

Chromite Paleoplacer in the Permian Sediments at the East Edge of the East European Platform: Composition and Potential Sources

Ildar R. Rakhimov [1,2,*], Evgenii V. Pushkarev [2] and Irina A. Gottman [2]

[1] Ufa Federal Research Center, Institute of Geology, Russian Academy of Science, Karl Marx Street, 16/2, 450077 Ufa, Russia

[2] A.N. Zavaritsky Institute of Geology and Geochemistry, Ural Branch, Russian Academy of Science, Academician Vonsovsky Street, 15, 620016 Yekaterinburg, Russia; pushkarev.1958@mail.ru (E.V.P.); gottman@igg.uran.ru (I.A.G.)

* Correspondence: rigel92@mail.ru; Tel.: +7-919-159-0904

Abstract: A chromite occurrence called the Sabantuy paleoplacer was discovered in the Southern Pre-Ural region, at the east edge of the East-European Platform in the transitional zone to the Ural Foredeep. A ca. 1 m-thick chromite-bearing horizon is traced at a depth of 0.7–1.5 m from the earth's surface for the area of ca. 15,000 m^2. The chromspinel content in sandstones reaches 30–35%, maximum values of Cr_2O_3 are 16–17 wt.%. The grain size of detrital chromspinel ranges from 0.15 to 0.25 mm. Subangular octahedral crystals dominate; rounded grains and debris are rare. The composition of detrital chromspinel varies widely and is constrained by the substitution of Al^{3+} and Cr^{3+}, Fe^{2+} and Mg^{2+} cations. Chemically, low-Al (Al_2O_3 = 12 wt.%) and high-Cr (Cr_2O_3 = 52–56 wt.%) chromspinel prevail. The compositional analysis using discrimination diagrams showed that most chromites correspond to mantle peridotites of subduction settings. Volcanic rocks could be an additional source for detrital chromites. It is confirmed by compositions of monomineralic, polymineralic and melt inclusions in chromspinels. The presented data indicates that ophiolite peridotites and related chromite ore associated with oceanic and island-arc volcanic rocks, widespread in the Ural orogen, could be the main sources of the detrital chromspinel of the Sabantuy paleoplacer.

Keywords: composition of chromspinel; solid-state inclusions; melt inclusions; chromite placer; provenance sources; ophiolite; Ural Foredeep; Ural orogen

Citation: Rakhimov, I.R.; Pushkarev, E.V.; Gottman, I.A. Chromite Paleoplacer in the Permian Sediments at the East Edge of the East European Platform: Composition and Potential Sources. *Minerals* **2021**, *11*, 691. https://doi.org/10.3390/min11070691

Academic Editor: Shoji Arai

Received: 25 May 2021
Accepted: 23 June 2021
Published: 27 June 2021

1. Introduction

Minerals of the spinel group show a wide range of solid solution series due to substitution of bivalent (Fe^{2+}, Mg, Mn, Ni, Zn) and trivalent (Fe^{3+}, Al, Cr) cations. They can crystallize in different magmatic, metamorphic and metasomatic rocks under various P-T-fO_2 conditions, which makes them critical petrogenetic indicators [1–5]. Magnetite and chromspinel are the most widespread minerals of the spinel group. Their high hardness, density (>4 g/cm^3) and resistance to weathering provide their accumulation in sedimentary rocks, where these minerals often become dominant in the heavy fraction and may produce placers [6–8]. The study of the composition of detrital chromspinel, as well as mineral and melt inclusions within them, allows interpreting the composition of protolith and, in some cases, the geological or geographic location of provenance sources [8–21].

The Upper Paleozoic sedimentary formations of the Late Devonian, Carboniferous and Permian Systems occurring at the east edge of the East European Platform and in the Ural Foredeep, were mainly produced by the accumulation of terrigenous material removed from the Ural orogen, which was situated eastward and completely finished its development at the end of Late Paleozoic [22–24]. The thickness of Upper Paleozoic sedimentary sequences approaches 12–15 km, and these rocks comprise large and giant oil, gas and salt deposits [25,26]. The Permian sediments contain numerous stratiform

Cu-sandstone deposits [27]. Usually, the heavy fraction of the Permian sandstones, which portion is commonly less than 0.4%, contains chromspinel, often as a dominant mineral [6].

The Hercynian Ural orogen stretches for 2500 km from the Aral Sea in the south to the Arctic Ocean. The geodynamic evolution of Urals embraced the Early Paleozoic continental rifting and formation of the oceanic basin accompanied by several volcanic island arcs and further ocean closure and a collision of island arcs with the East European continental margin and then to the collision with the Kazakhstan craton in the Late Paleozoic [22–24]. Mafic-ultramafic complexes and intrusions with accessory and ore chromite mineralization were formed at all stages of this evolution. During the Pre-Uralian cratonic stage, the layered gabbro–peridotite intrusions and numerous picritic and dolerite dykes were formed [22,28]. During the oceanic and island-arc stages of Urals development in the Lower and Middle Paleozoic, ophiolites, huge masses of volcanic rocks and dunite–clinopyroxenite–gabbro intrusions of Uralian-Alaskan-type of the world-largest Ural Platinum Belt were formed [24,29–34]. The Late Paleozoic collision produced an orogeny with several submeridional tectonic zones [23,24] (Figure 1a,b). Fragments of the oceanic lithosphere and island arc terranes were preserved in some synforms or exhumed to the earth's surface along the Main Uralian Fault and other tectonic sutures during the Late Paleozoic closure of ocean and tectonic shortening [24,29–31]. Peridotites of the most ophiolite complexes in the Urals host numerous minor, major and unique chromite deposits [35]. Serpentinite debris, chromspinel and other products of erosion of ophiolites and different mafic–ultramic complexes have contributed to sedimentary deposits westward of the Ural orogen since the Upper Devonian [6]. However, no economically important chromite placers of the Paleozoic or younger age have been discovered yet, except for some minor slope deluvial placers spatially associated with ultrabasic massifs [36].

Recently, a chromite paleoplacer called the **Sabantuy** ore occurrence has been first discovered in the Permian deposits of the south-eastern margin of the East European Platform in the transition area to Ural Foredeep [37]. It occurs as a placer at least 250 m long in the meridional direction and ca. 50 m wide; the thickness of chromite-bearing sandstones is ca. 1 m. Ore sandstones, called the chromitolites, contain up to 30–35% of chromspinel and 20–25% of iron-titanium oxides, i.e., ilmenite, titanomagnetite, hematite, rutile, ferropseudobrookite, etc. The bulk Cr_2O_3 content is up to 17.2 wt.%. The provenance source of the Sabantuy paleoplacer is not clear, though there was a suggestion that some material was derived from the Uralian ophiolites [37].

The current paper presents results of detailed lithological, mineralogical and geochemical studies of the Sabantuy paleoplacer that provide a ground for assumed sources for chromspinel.

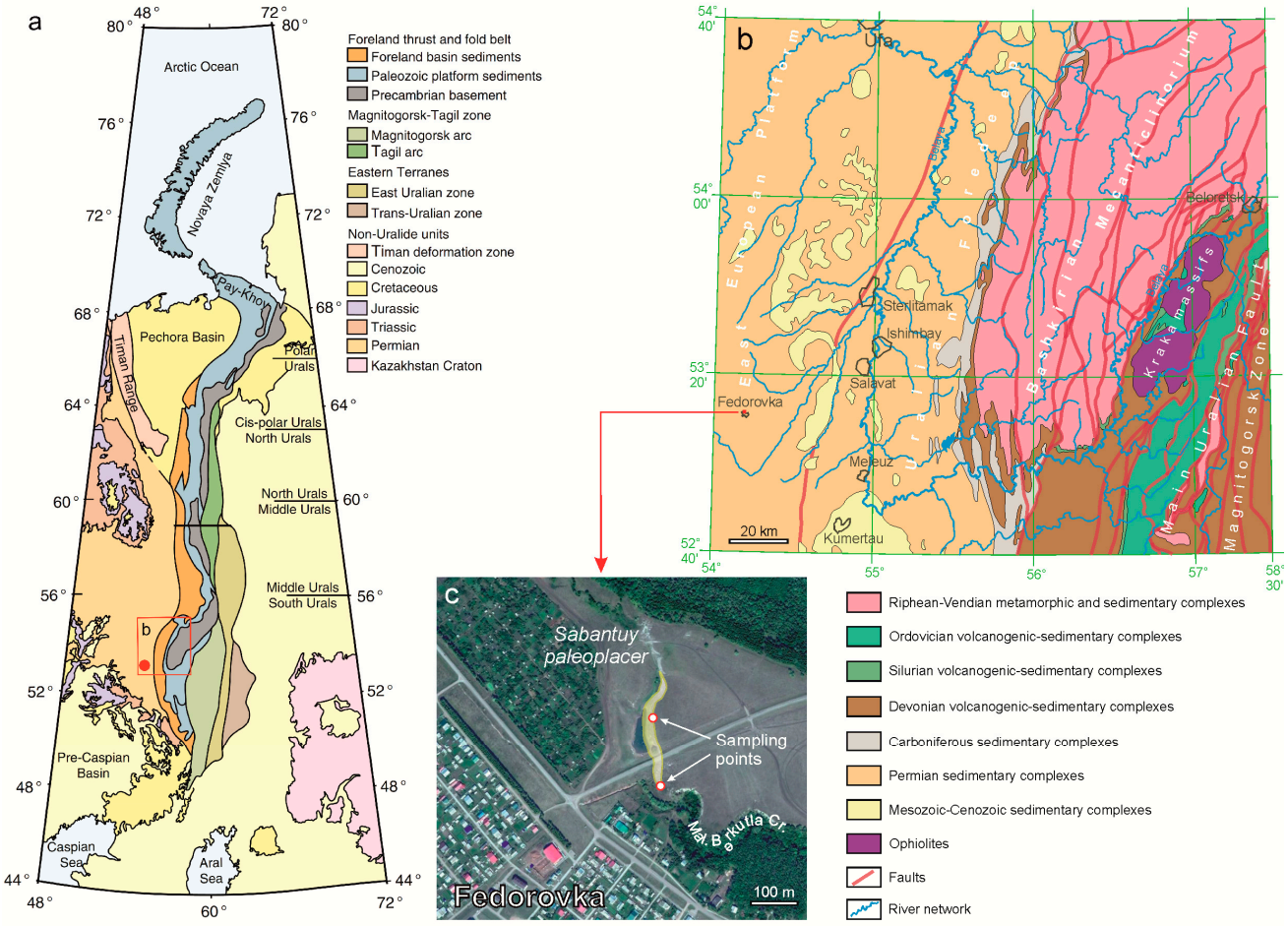

Figure 1. Structural zones of the Uralides [23] (**a**) with the position of Sabantuy placer close to Fedorovka village (red rectangle) corresponding the fragment of the State geological map N-40 (Ufa) simplified after Knyazev with co-authors [38] (**b**). The Sabantuy paleoplacer locality on a satellite image (**c**).

2. Sabantuy Placer Locality and Geological Settings

The Sabantuy ore occurrence was discovered on the left coast of Malaya Berkutla Creek in the southwest of the Fedorovka village, 200 km south-southwest of the Ufa, the Republic of Bashkortostan (Figure 1b). The chromite-bearing horizon is seated at a depth of 0.7–1.5 m from the earth's surface. According to verified data, the ore occurrence is traced in the meridional direction for the distance of 300 m and the width of at least 50 m. Further research is required to specify the placer parameters. Towards the north, sandstones and the chromite-bearing horizon are overlapped by a sequence of Permian limestones and brown Neogene loesses. The chromite-rich sandstones and overlapping and underlying sedimentary rocks were collected in artificial open pits and trenches along the Malaya Berkutla Creek.

The section available for observation is represented (Figure 2, from top to bottom) by: (1) light grey and brown marly limestones (0.5 m); (2) grey fine-grained cross-bedded sandstones (0.5 m); (3) dark-colored cross-bedded chromite sandstones (1 m); (4) grey cross-bedded sandstones with conglomerate interlayers (8 m); (5) brownish-grey horizontally bedded sandstones (12 m); (6) greenish-grey horizontally bedded siltstones and mudstones ($\geq$3 m).

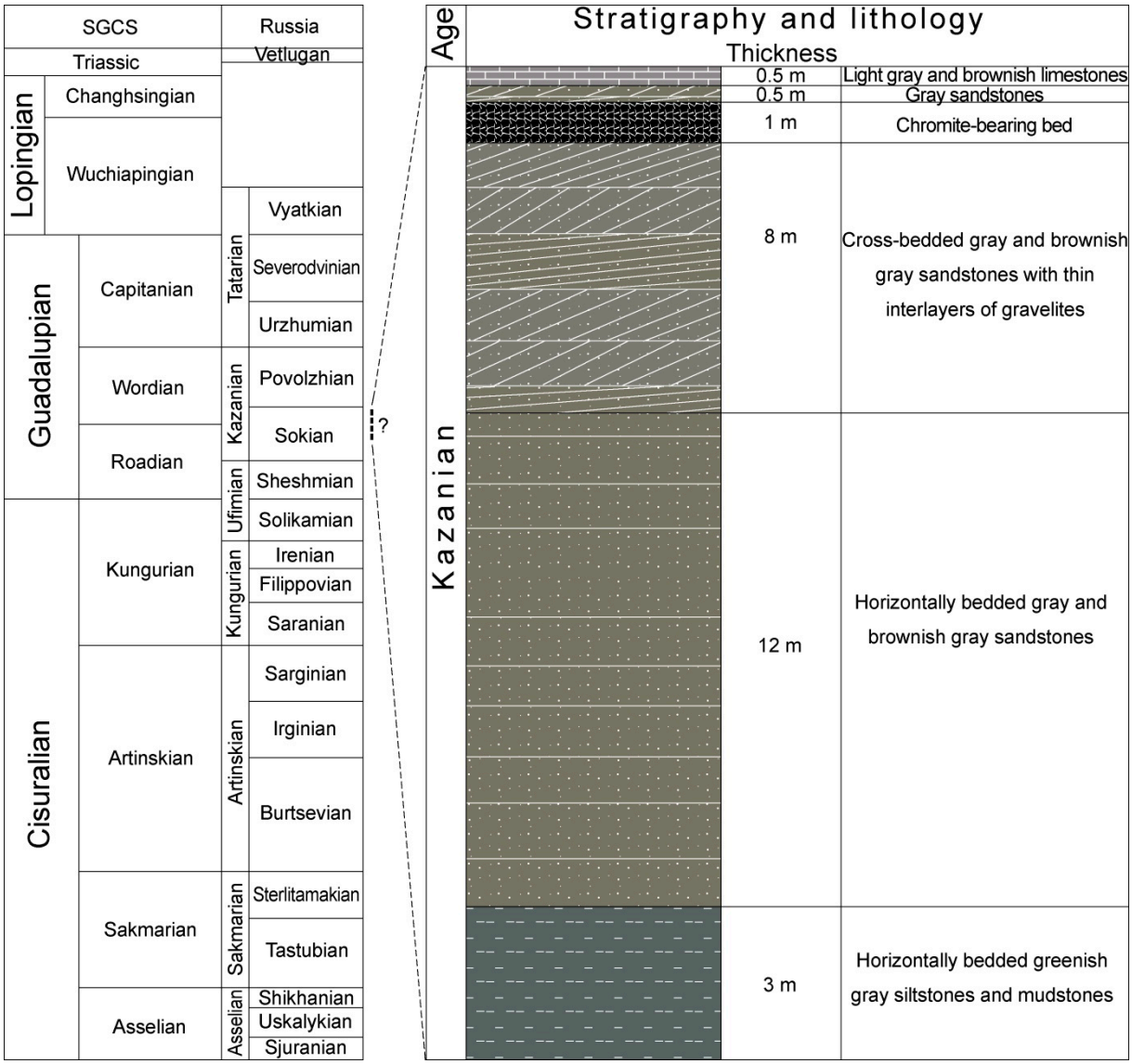

Figure 2. Stratigraphic and lithological chart of the Sabantuy paleoplacer cross-section (**right**) with a comparison to the Standard Global Chronostratigraphic Scale (SGCS) and the General Stratigraphic Scale of Russia [39] (**left**).

The above stratigraphic sequence is a part of carbonate-terrigenous sediments of the Kazanian Stage of the Permian System, which is correlated with the Late Roadian and Wordian Stages of the International Stratigraphic Chart [39] (Figure 2). According to [37], the sediments of the Kazanian stage of the Southern Pre-Urals occur on an eroded surface of red-colored sediments of the Ufimian Stage. It is subdivided into the Lower Kazanian (P_2kz_1) and Upper Kazanian (P_2kz_2) Substages. The former substage is represented by greenish-grey siltstones, mudstones with limestone interlayers and sandstones with gritstone lenses totally as thick as ca. 50–70 m. The latter substage is represented by continental (red-colored clays, sandstones) and marine (grey-colored clays, sandstones with limestones) sediments with a total thickness of 35–60 m. The age of sediments is validated by ostracodes (Darwinula alexandrinae, Darwinula sentjakensis Sharap., Monoceratina fastiglata Kotsch, etc.) and foraminifers (Gavellina Grandis Schneid., C. unica Kotsch., Amphissites tscherdynzevi Posn., etc.) found in interlayers of marls and limestones [37]. The paleogeographic settings of sedimentation at the Kazanian Stage corresponded to the shallow sea environment with a transition to the continental conditions. Available data suggest that the studied section with chromite sandstones can be compatible with

the upper part of the Lower Kazanian Substage. Next, it can be correlated to the Sokian horizon of the Russian General Stratigraphic Scale and the Early Wordian of the SGCS (Figure 2).

3. Analytical Methods

Mineralogical investigations have been carried out using four representative samples of chromite-rich sandstone from the Sabantuy paleoplacer. Rocks were crushed, sifted through a 0.5 mm sieve, cleaned from the dust and firstly studied under a binocular microscope. We have handpicked at least 30–40 grains of chromspinels and their intergrowth with sandstone matrix from each sample for the studding of external shapes of grains and crystals using SEM Jeol-6390LV (JEOL Ltd., Tokyo, Japan). More than 800 grains of opaque minerals from these four samples (more than 200 grains for each) were mounted in epoxy resin and polished. Most of these grains are chromspinel, but titanomagnetite, ilmenite and other minerals are also present. The total amount of chromspinel grains plus few other oxide phases, studied by X-ray microprobe, approaches 250 grains, but for the next investigations, we used 218 grains. Solid-state, polymineralic and re-crystallized melt inclusions in chromite have been studied using the SEM Jeol-6390LV with EDS Oxford spectrometer and Cameca SX-100 X-ray microprobe in the Scientific Center "Geoanalitik," Institute of Geology and Geochemistry, Ural Branch, Russian Academy of Sciences (Yekaterinburg, Russia). Measurement conditions were as follows: the pressure in the chamber of samples is 6×10^{-4} Pa; the accelerating voltage was 15 kV; the current strength was 30 nA; the diameter of the electron beam was 5 μm on the sample. Pyrope, rutile, jadeite, chromite, garnet, diopside and orthoclase were used as standards. To determine all peaks, the most intense $K\alpha$ lines were used. Na, Mg, Al and Si were measured on TAP crystals; K and Ca on LPET crystal; Mn, Ti, Fe and Cr on LIF. The time of pulse acquisition at peaks of analytical lines is two times longer than the time of pulse acquisition at the background on both sides from the peak and was 10 s for all elements. Standard deviation (wt.%) varies from 0.24 to 0.30 for Si; from 0.03 to 0.10 for Ti; from 0.03 to 0.25 for Al; from 0.06 to 0.10 for Cr; 0.15 to 0.71 for Fe; from 0.06 to 0.36 for Fe; from 0.08 to 0.18 for Mg; from 0.04 to 0.22 for Ca; from 0.02 to 0.07 for Na; and from 0.01 to 0.03 for K.

The chemical composition of rocks was determined by Carl Zeiss VRA-30 XRF spectrometer with tungsten-anode at the Institute of Geology of the Ufa Federal Research Center (Ufa, Russia). The accelerating voltage was 30–40 kV; the current strength was 400 mA. The detection limit for SiO_2 and Al_2O_3 was 0.2 wt.%; for TiO_2, FeO, Cr_2O_3, MnO, CaO, K_2O and P_2O_5, it was0.01 wt.%; for S, it was 0.005 wt.%. Russian State reference materials (chromium ores PT-9 (Cr_2O_3 56.2 wt.%), K-2 (Cr_2O_3 34.3 wt.%), ХБ-1 (Cr_2O_3 19.0 wt.%) were used for the calibration of analytical lines. The "Lost of ignition" (LOI) was determined using a standard method. One gram of previously dried and weighted sample heated up to 1000 °C and keep it for about 1 h for the stabilization of mass. The difference between mass divided by the mass of the sample, multiplied by 100%, gave the LOI.

The calculated ratios for chromspinel are: Cr# = Cr/(Cr + Al) and Mg# = Mg/(Mg + Fe^{2+}).

4. Results

4.1. Lithology and Petrography

The chromite-bearing horizon is represented by alternating layers of chromitolites (chromite-rich sandstone) and grey chromite-depleted sandstones. The thickness of chromitolite layers ranges from 1 mm to 13 cm. They clearly mark the texture of sediments that combines horizontal and cross-bedding (Figure 3a,b). The deposits typically have quasisymmetric undulation ripples and signs of wave ripples as curved and branching ridgelets. Interaction of layered series is referred to as the non-parallel truncated convex type. Observations indicate that ore bodies are not persistent in lateral and get early replaced by barren sandstones, alternating subsequently.

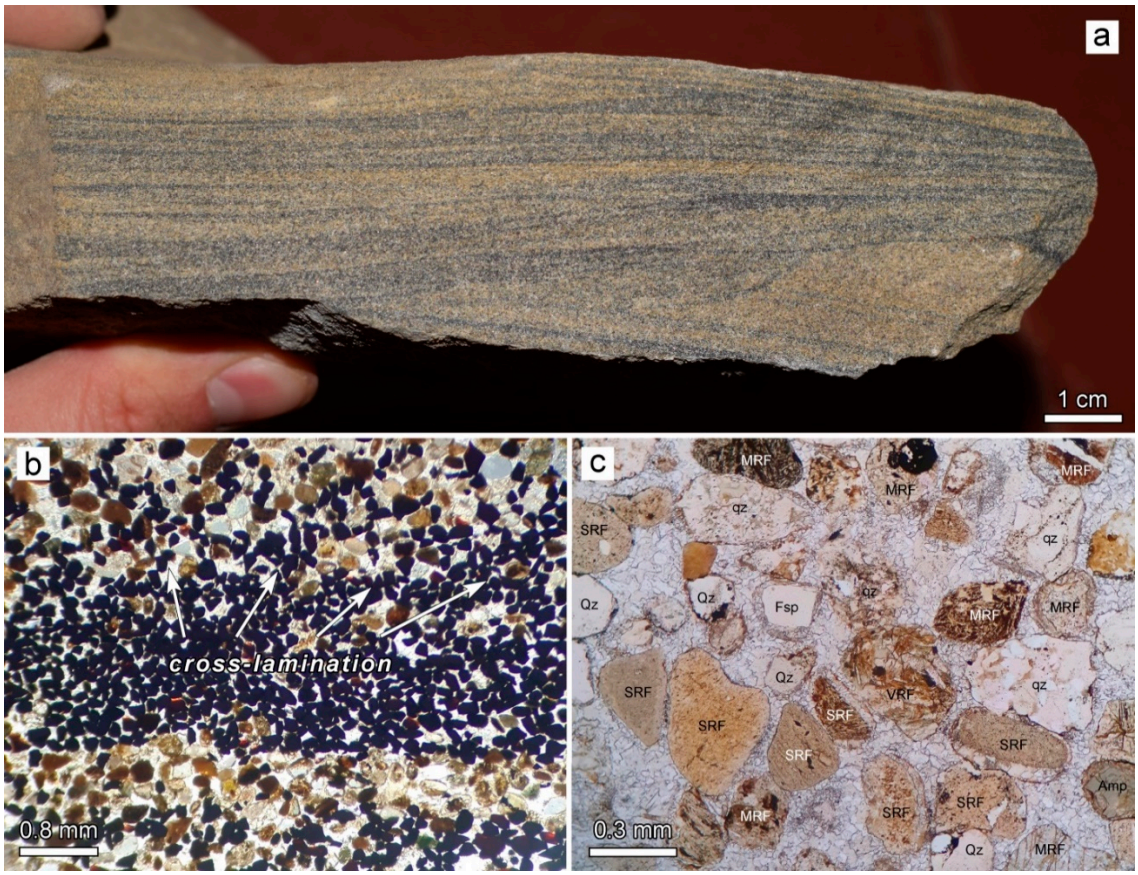

Figure 3. Hand size sample of chromite-rich sandstone from Sabantuy paleoplacer (**a**); (**b**) photomicrograph of chromitolite layer with cross-lamination texture (plane polarized light); (**c**) photomicrograph of the clastic texture of underlying sandstones (plane polarized light). Amp—amphibole, Fsp—feldspar, MRF—fragments of metamorphic rock, Qz—quartz, qz—quartzite, SRF—fragments of sedimentary rock and VRF—fragments of volcanic rock.

Debris in grey sandstones (Figure 3c) is represented by fine fragments of rocks (50–80%), quartz (6–15%), silicate minerals (4–9%, pyroxene, amphibole, plagioclase, chlorite, mica, titanite) and ore minerals (1–12%, chromspinel, magnetite, ilmenite, etc.) (Figure 3b). Rock debris contains prevalent metamorphic quartzites and schists (53–66%), as well as fragments of sedimentary (32–46%) and magmatic rocks (1–3%). Serpentinite debris is commonly minor. Sandstones are well-sorted, and their fragments range from 0.2 to 0.4 mm in size (fine-grained sandstone fraction); the grains are rounded with a varying degree, but mainly poorly (1–2 scores on the Russell and Taylor scale [40]). The matrix of sandstones is represented mostly by fine-grained calcium carbonate with pelitomorphic texture, sometimes porous. The volumetric fraction of cement is 35–45%. Sandstones underlying the ore-bearing horizon are relatively low in fragments of silicate (1–2%) and ore minerals (0–1%) and magmatic rocks (0.1–0.6%) while overlying sandstones contain up to 2–4% of silicate minerals, 13–22% of opaque minerals and 5–13% of magmatic rocks debris. According to the composition of debris, sandstones are classified as lithite greywackes–phyllarenites (Figure 4).

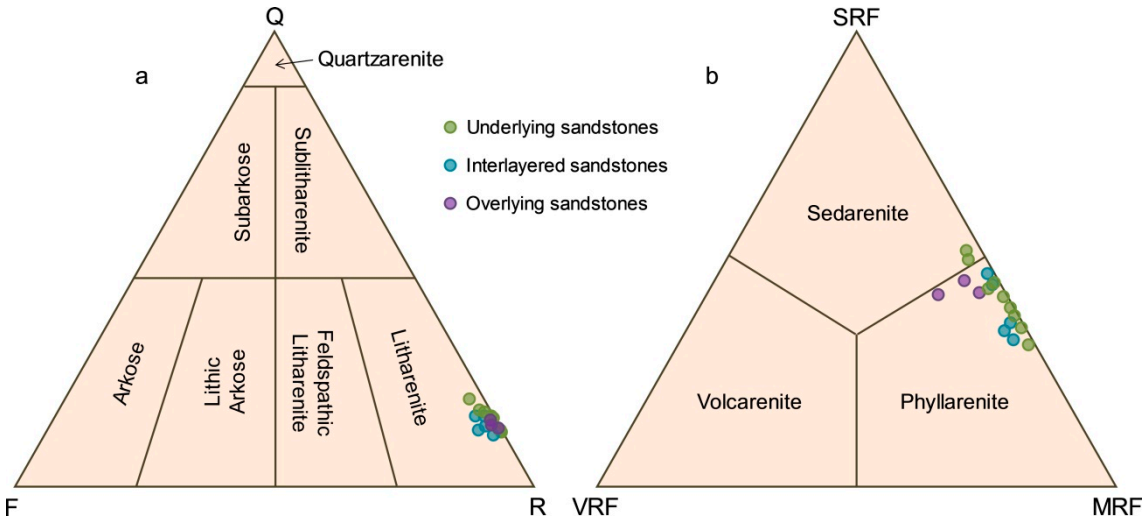

Figure 4. Ternary classification diagrams Q–F–R (Quartz–Feldspar–Rock fragments) (**a**) and SRF–VRF–MRF (Sediment rock fragments–Volcanic rock fragments–Metamorphic rock fragments) (**b**) after [41] for Sabantuy sandstones.

4.2. Chemical Composition of Sandstones

The petrographic studies show that the composition of sandstones is mainly defined by proportions between the debris of metamorphic and sedimentary rocks, opaque minerals (chromspinel, ilmenite, magnetite) and carbonate matrix. The studied sandstone samples can be divided into three groups based on their visual properties and the content of Cr_2O_3 (wt.%): (1) chromite-free (barren, from the underlying bed), $Cr_2O_3 < 0.1$, (2) chromite-bearing grey sandstones with rare interlayers of chromitolites, $Cr_2O_3 = 1.6–2.7$, (3) chromite-rich (ore sandstones) containing numerous chromite-rich layers, $Cr_2O_3 = 10.6–16.6$ (Table 1). Sandstones of the first and second groups show weakly variations of SiO_2, CaO, FeO_t and Cr_2O_3 (Table 1). Chromitolites have high variations of SiO_2 (4.0–29 wt.%), CaO (13–29 wt.%), FeO_t (7.4–21.6 wt.%) and TiO_2 (1.0–6.8 wt.%). However, all of the studied samples in total yield a relatively sustained Al_2O_3 content (4–7 wt.%). Rocks of the first and second groups tend to show a clear negative correlation between Cr_2O_3 and SiO_2, but in chromitolites, it is between Cr_2O_3 and CaO (Figure 5a,b). The prevalence of carbonate in the rock matrix explains the extremely high LOI. All rock types show a positive correlation between the Cr_2O_3 and TiO_2 content, although chromitolites produce two individual trends (Figure 5c). Different trends are also observed in the TiO_2–Cr_2O_3/TiO_2 diagram, where one subgroup is characterized by a clear negative correlation, whereas the other subgroup shows an almost constant Cr_2O_3/TiO_2 ratio independent of TiO_2 content in bulk rock composition (Figure 5c). It indicates a different pattern of chromspinel and iron-titanium minerals accumulation in sediments, but the nature of this phenomenon requires further investigation. Barren and chromite-bearing sandstones, on the contrary, show a positive correlation between the titanium and chrome-titanium ratio. A positive correlation is also recorded for the content of FeO_t and Cr_2O_3, though the direction of the trends differs in chromitolites and sandstones of the first and second groups (Figure 5e). The FeO_t–TiO_2 plot yields a single positive trend for all samples (Figure 5f). Extrapolation of this trend intersects compositions of titanomagnetites with an extremely high TiO_2 value (up to 20 wt.%), recorded among minerals of the heavy fraction. Ilmenite is also present in the heavy fraction, but data points representing the composition of this oxide are far above the trend and should not influence its direction. We can suggest that the titanium content in sandstones is mainly linked to the accumulation of titanomagnetite.

Table 1. Bulk chemical composition of the Sabantuy chromite paleoplacer sandstones and ores (wt.%).

#	Sample	SiO_2	TiO_2	Al_2O_3	FeO_t	Cr_2O_3	MnO	MgO	CaO	Na_2O	K_2O	P_2O_5	S	LOI	Total
1	D_3-4	4.40	4.32	5.04	15.55	12.07	0.35	14.34	23.81	3.00	0.08	0.07	0.04	13.98	97.05
2	D_3-5	4.87	6.83	5.64	19.54	16.55	0.48	16.48	13.00	2.00	0.10	0.12	0.07	13.99	99.65
3	D_5-13-ai	4.03	5.25	5.55	21.24	15.02	0.19	11.19	20.54	0.10	0.03	0.10	0.07	16.55	99.86
4	D_5-13-as	4.09	4.73	5.03	21.60	14.07	0.18	12.86	23.51	0.10	0.03	0.09	0.06	11.75	98.10
5	D_5-14a	24.60	0.65	4.10	4.48	1.60	0.19	10.30	28.69	0.47	0.17	0.07	0.02	24.36	99.70
6	D_5-14b	20.91	0.89	3.99	5.32	2.68	0.19	10.72	28.77	0.53	0.12	0.07	0.01	24.49	98.69
7	D_5-14bx	22.35	0.80	4.87	4.72	2.10	0.17	10.24	28.58	0.52	0.12	0.08	0.02	24.65	99.20
8	D_5-18a	17.91	2.80	6.93	13.52	16.06	0.14	5.18	18.87	0.60	0.08	0.04	0.04	16.87	99.03
9	D_5-19	29.66	0.24	5.30	3.16	0.03	0.18	6.50	25.99	0.64	0.20	0.06	0.04	27.03	99.03
10	F_{19}-1	18.06	2.26	5.63	12.90	14.96	0.13	2.12	24.60	0.64	0.08	0.05	0.04	17.61	99.08
11	F_{19}-2	29.03	0.98	5.15	7.36	10.64	0.10	4.35	22.86	0.61	0.20	0.05	0.03	17.52	98.88
12	F_{19}-5	13.17	1.37	3.98	10.52	10.91	0.10	6.00	29.19	1.35	0.11	0.06	0.03	22.50	99.29
13	F_{19}-7	27.01	0.24	4.66	3.24	0.06	0.17	3.68	31.21	1.54	0.17	0.08	0.04	26.95	99.05

Note: 1–4, 8, 10–12—ore sandstones (chromitolites), 5–7—chromite-bearing interlayered sandstones, 9, 13—chromite-free underlying sandstones; FeO_t = FeO + Fe_2O_3.

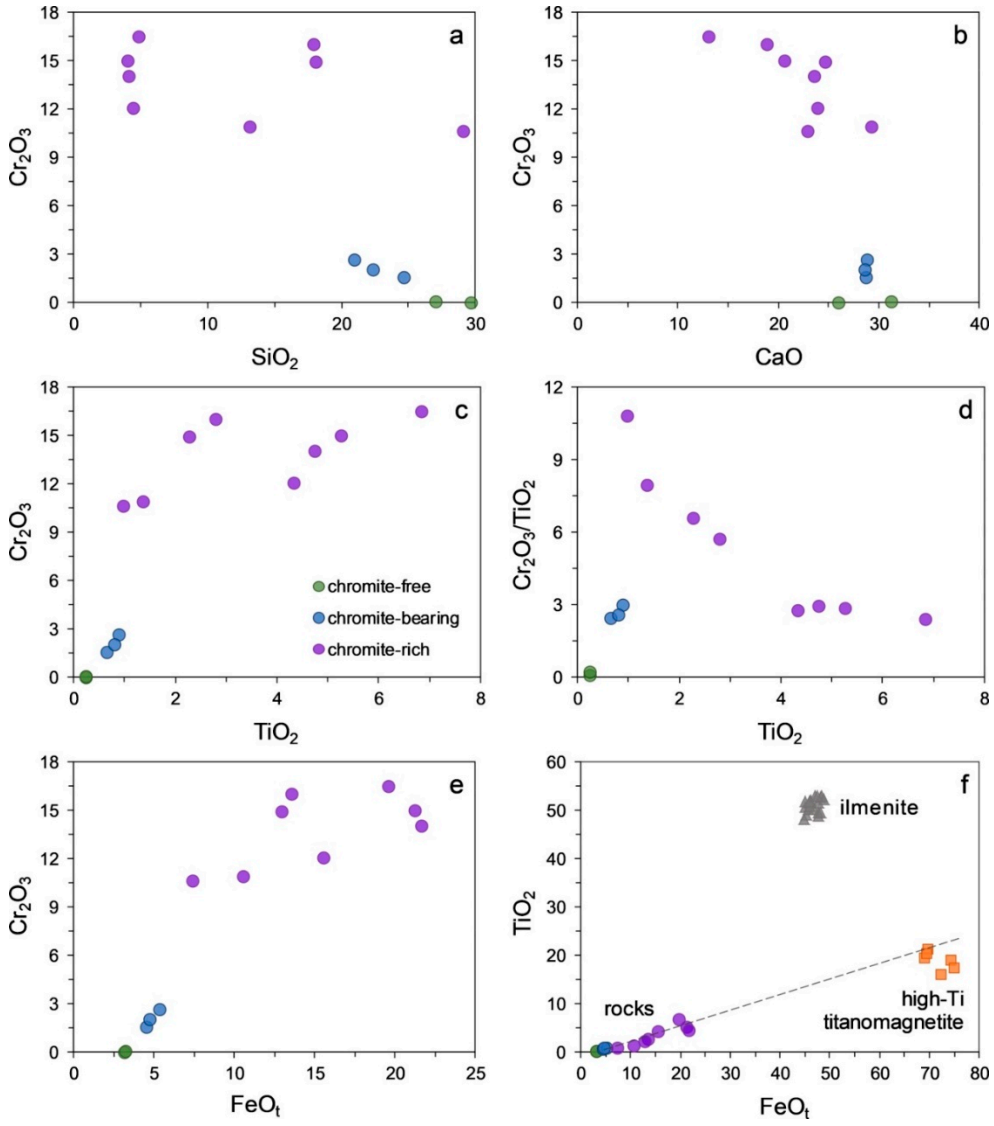

Figure 5. Binary diagrams for chromite-free, chromite-bearing and chromite-rich sandstones, ilmenite and high-Ti titanomagnetite from Sabantuy paleoplacer (in wt.%): SiO_2 vs. Cr_2O_3 (**a**), CaO vs. Cr_2O_3 (**b**), TiO_2 vs. Cr_2O_3 (**c**), FeO_t vs. Cr_2O_3/TiO_2 (**d**), FeO_t vs. Cr_2O_3 (**e**), FeO_t vs. TiO_2 (**f**). Note: FeO_t = FeO + Fe_2O_3.

4.3. Morphology of Chromspinel Grains

The size of chromspinel grains in the studied samples ranges from 0.15 to 0.25 mm. Grains commonly occur as idiomorphic, well-facetted crystals of octahedral shape. Crystal fragments are also present. The following groups of chromspinel grains can be defined based on their morphological features: (1) octahedral crystals with different defects of facets (elements of incomplete growth, dendritic surface, induction surface) (Figure 6a–c); (2) distorted octahedral crystals with a flattened shape, additional facets (including vicinals) and different defects of facets (Figure 6d,e); (3) non-octahedral crystals or irregular-shaped rounded crystals with numerous defects of the surface (corroded or abraded surface?) (Figure 6f,g); (4) crystal fragments, mainly non-octahedral (Figure 6h). Most of the studied grains belong to the first and second groups. Clastic grains occur as crystal fragments (rhombic dodecahedron?) 2–3 times larger than crystals of the 1–3 groups. The mechanic abrasion of chromspinel grains during the transfer and sedimentation is poorly observed.

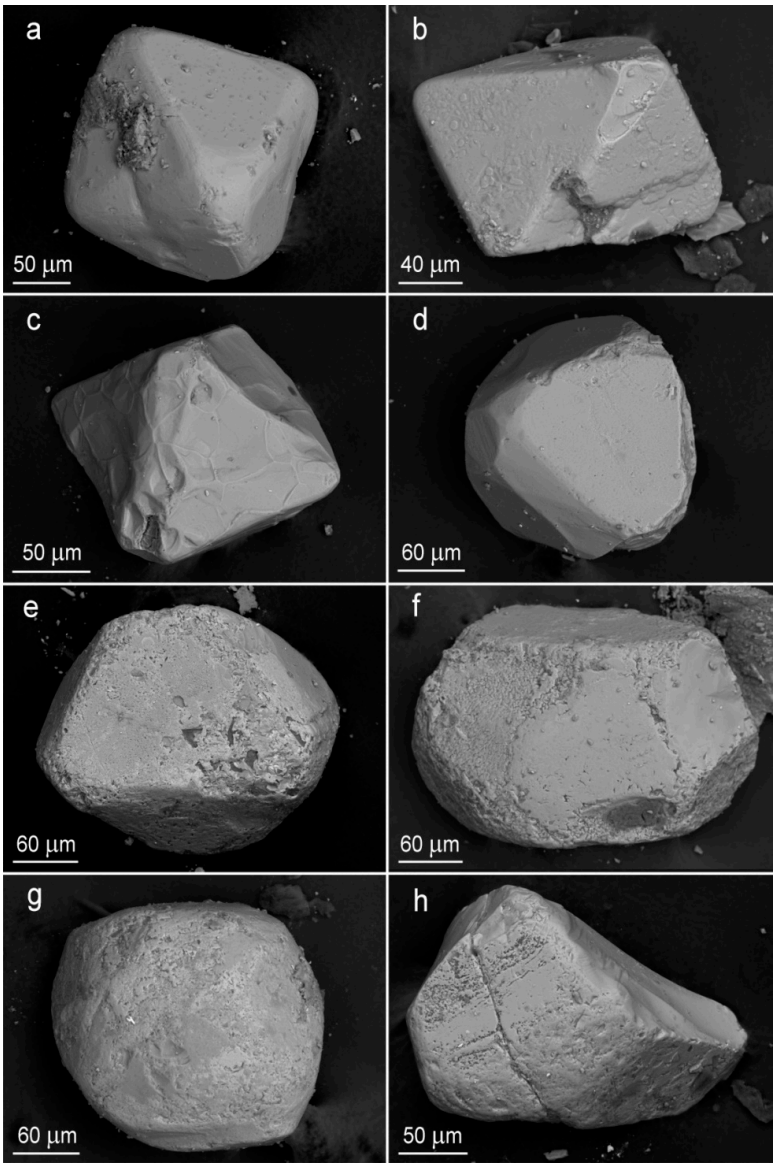

Figure 6. BSE images of chromspinel grains from chromitolites of Sabantuy paleoplacer: (**a**–**c**) octahedral, (**d**) octahedral with vicinal faces, (**e**) flattened octahedral, (**f**) non-octahedral (rhombododecahedron) corroded, (**g**) rounded non-octahedral (myrihedron) corroded and (**h**) fragments of non-octahedral crystal.

In polished sections, chromspinel sometimes demonstrates a fractured texture (Figure 7a) and weak zonation. Among the grains, the following types of zoning and heterogeneity can be identified: (a) unclear concentric zoning with a secondary magnetite rim (Figure 7b) and (b) mottled zoning or texture (Figure 7c,d). Grains with a porous structure also occur (Figure 7d). Grains are angular and subangular mostly, less often subrounded.

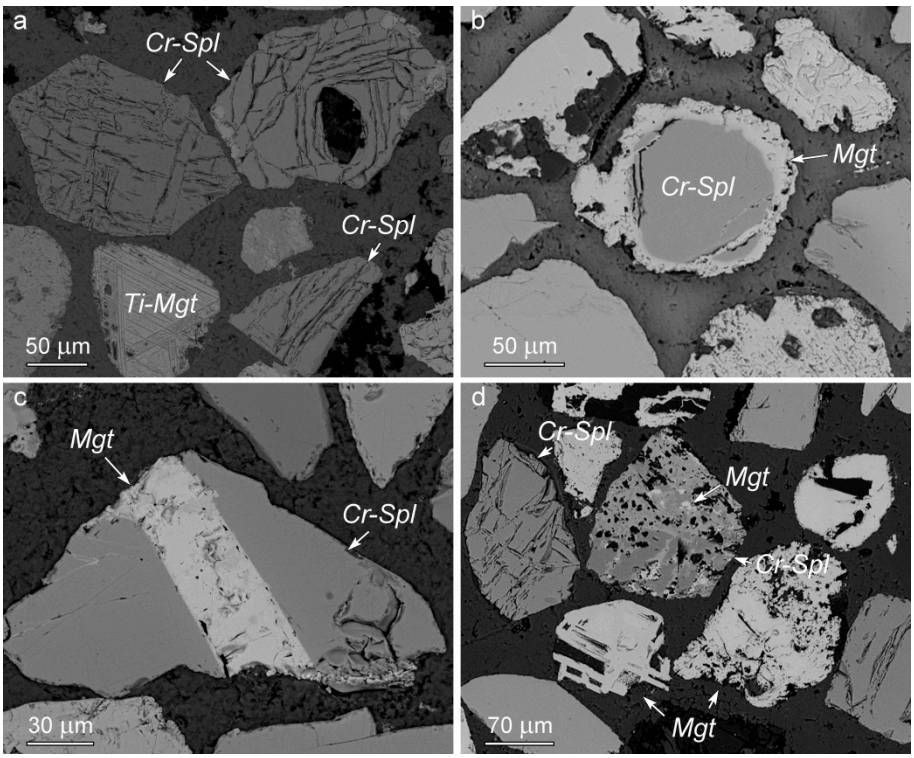

Figure 7. BSE images of chromspinels in a polished section of chromitolites from Sabantuy paleoplacer: (**a**) fractured grains, (**b**) grain with secondary magnetite rim, (**c**) grain with magnetite band and (**d**) patchy and spongy structure grain. Note: Cr-Spl—chromspinel, Mgt—magnetite and Ti-Mgt—titanomagnetite.

4.4. Composition of Chromspinel

The composition of detrital chromspinel from the Sabantuy paleoplacer varies widely (wt.%): Cr_2O_3 9.9–65.5, Al_2O_3 0.1–47.3, FeO 11.6–81.6 and MgO 1.5–18.3 (Table 2, Supplementary Table S1). No significant differences in chemical compositions of chromspinel were detected for studied samples. No regular differences in composition for more rounded and less rounded grains were defined either. Notably, in almost all cases, statistical processing of the chemical compositions of studied chromspinel indicates a unimodal lognormal distribution of components (Figure 8), which allows defining the prevalent chromite type. Thus, major data on the Cr_2O_3 content show 52–56 wt.% (Figure 8a), and Al_2O_3 shows 10–14% with the distinct maximum at 12% (Figure 8c). The statistical maximum for the Cr# is 0.7–0.8 (Figure 8b). The studied chromspinels are characterized by a very low titanium content, i.e., the distinct max TiO_2 content in the histogram corresponds to the interval of 0.1–0.2 wt.%. Chromspinel grains with the TiO_2 content of ca. 1% and more are rare (Figure 8d). The statistical maximum in histograms for MgO is 11 wt.%, and for Mg#, it is 0.55–0.65 (Figure 8e,f). FeO content in detrital chromspinel varies in the range of 15–30 wt.% with the statistical maximum in between 18–27 wt.% on the distribution histogram (Figure 8g). In addition, chromspinels are characterized by a statistically low degree of the iron oxidation state, i.e. $Fe^{3+}/(Fe^{2+} + Fe^{3+})$ is commonly <0.2 (Figure 8h). Manganese, nickel, zinc and vanadium show statistically low concentrations that become significant in single grains only, but even in these cases, the concentrations of these ele-

ments are less than 0.8 wt.%. The average chromspinel composition in the total selection of 205 analyses is the following (wt.%): Cr_2O_3 = 49, Al_2O_3 = 17, FeO_t = 22, MgO = 11, TiO_2 = 0.16, Cr/(Cr + Al) = 0.7 and Mg/(Mg + Fe^{2+}) = 0.5. These values slightly differ from the compositions typical of maximums in histograms due to the lognormal distribution of components. Most of the studied grains have no distinct zonality. A weak zonality was rarely traced as decreased Mg/(Mg + Fe^{2+}) and the chromium content at the very rim of grains.

Table 2. Selective microprobe analyses of chromspinel from the Sabantuy paleoplacer (wt.%).

#	TiO_2	Al_2O_3	Cr_2O_3	V_2O_3	FeO	MnO	MgO	NiO	ZnO	CaO	Total
1	0.09	17.68	50.42	0.22	19.81	0.22	10.54	0.07	0.16	0	99.21
2	0.04	5.76	65.06	0.04	17.09	0.05	12.55	0.08	0.12	0.01	100.79
3	0.17	30.2	37.85	0.24	17.68	0.05	13.79	0.15	0.15	0	100.28
4	0	47.33	18.22	0.11	17.07	0.07	16.27	0.29	0.21	0.02	99.58
5	0.1	23.48	43.49	0.3	19.86	0.1	12.79	0.11	0.1	0	100.33
6	0.09	10.53	60.89	0.08	15.7	0.04	12.72	0.08	0.12	0.01	100.25
7	0.07	13.97	53.94	0.21	20.91	0.06	10.19	0.07	0.21	0	99.63
8	0	5.1	61.65	0.34	24.3	0.27	5.6	0.01	0.29	0.06	97.56
9	0.06	7.03	64.19	0.11	13.33	0	14.57	0.18	0	0	99.47
10	0.09	6.87	65.31	0.13	14.03	0	13.66	0.07	0.09	0.02	100.25
11	0.11	10.35	58.43	0.25	23.04	0.23	7.85	0.04	0.31	0	100.61
12	0.17	0.1	20.21	0.14	72.08	0.44	1.63	0.41	0.15	0.07	95.33
13	0.01	39.32	27.99	0.12	15.7	0.06	15.94	0.2	0.23	0	99.57
14	0.03	15.16	55.68	0.19	14.11	0.1	13.14	0.1	0.14	0	98.65
15	0.05	15.47	55.86	0.22	14.44	0.02	12.98	0.12	0.05	0.05	99.21
16	0.06	12.07	57.41	0.23	18.92	0.19	9.96	0	0.06	0	98.9
17	0.32	28.95	37.21	0.14	17.18	0.11	15.89	0.16	0.19	0.01	100.17
18	0.46	8.01	55.97	0.09	23.55	0.26	9.89	0.04	0.22	0.04	98.49
19	0.38	14.29	52.65	0.2	22.55	0.2	10.1	0.09	0.01	0.04	100.47
20	0.08	32.51	33.24	0.18	19.54	0.16	13.92	0.09	0.14	0	99.86
21	0.52	10.33	51.44	0.17	28.41	0.19	7.73	0	0.24	0.01	99.03
22	0.01	28.7	40.17	0.09	15.85	0.09	14.97	0.15	0.06	0.02	100.09
23	0	32.95	36.41	0.16	14.59	0.08	15.06	0.1	0.07	0.03	99.42
24	0.28	0.08	9.93	0.09	81.61	0.33	1.83	0.81	0	0.02	95.01
25	0.07	21.78	47.22	0.25	19.6	0.25	10.36	0	0.29	0	99.82
26	0.05	19.02	52.57	0.11	14.87	0.03	13.06	0.05	0.18	0	99.94
27	0.14	7.89	61.06	0.11	20.08	0.24	9.77	0.05	0.06	0.01	99.4
28	0.16	7.72	59.33	0.1	18.66	0.06	13.03	0.05	0.02	0	99.13
29	0.32	14.51	51.03	0.14	22.53	0.16	9.78	0.03	0.1	0.01	98.6
30	0.07	16.53	51.88	0.21	22.78	0.46	7.74	0	0.34	0.02	100.01
31	0.06	5.39	64.37	0.09	19.52	0.09	9.98	0.06	0.12	0.01	99.68
32	0	29.51	40.59	0.11	12.82	0.07	16.13	0.13	0.05	0	99.41
33	0.01	32.82	35.93	0.2	16.65	0.07	13.77	0.11	0.25	0.01	99.81
34	0	7.03	63.05	0.09	19.29	0.17	9.25	0.09	0.14	0.01	99.11
35	0.08	12.16	55.95	0.14	20.09	0.25	10.37	0.1	0.1	0	99.24
36	0.24	15.42	41.83	0.17	31.63	0.2	8.46	0.11	0.31	0	98.37
37	0.03	41.57	24.55	0.11	15.38	0.12	17.68	0.28	0.09	0	99.81
38	0	18.01	51.79	0.29	19.13	0.16	11.1	0.07	0.19	0	100.74
39	0.07	11.37	59.78	0.12	15.2	0.06	12.11	0.07	0.04	0	98.82
40	0.06	28.39	39.4	0.14	16.93	0.12	14.52	0.15	0.06	0	99.77
41	0.42	11.59	51.66	0.2	26.58	0.17	8.71	0.04	0.08	0	99.45
42	0.06	5.89	61.15	0.05	28.19	0.3	4.14	0.05	0.01	0	99.84
43	0.12	5.13	63.36	0.09	22.09	0.17	8.87	0.04	0.07	0	99.94
44	0.05	7.32	61.43	0.1	21.16	0.1	9.42	0.03	0.11	0.01	99.72
45	0.34	40.43	25.71	0.15	14.08	0.07	18.04	0.27	0.03	0.01	99.21
46	0.05	7.02	65.48	0.19	17.14	0.1	10.23	0.04	0.11	0	100.36
47	0.18	9.27	54.1	0.17	25.77	0.15	9.02	0.02	0.09	0.02	98.77
48	0.4	19.07	47.14	0.15	20.47	0.13	12.42	0.15	0.24	0	100.17
49	0.2	37.86	29.22	0.15	14.29	0.1	16.13	0.24	0.22	0	98.41
50	0.18	7.65	60.01	0.08	21.96	0.18	10.17	0.05	0.04	0.01	100.32

Note: 1–12—sample D_5-13, 13–24—sample D_5-18, 25–37—sample F_{19}-1, 38–50—sample F_{19}-3.

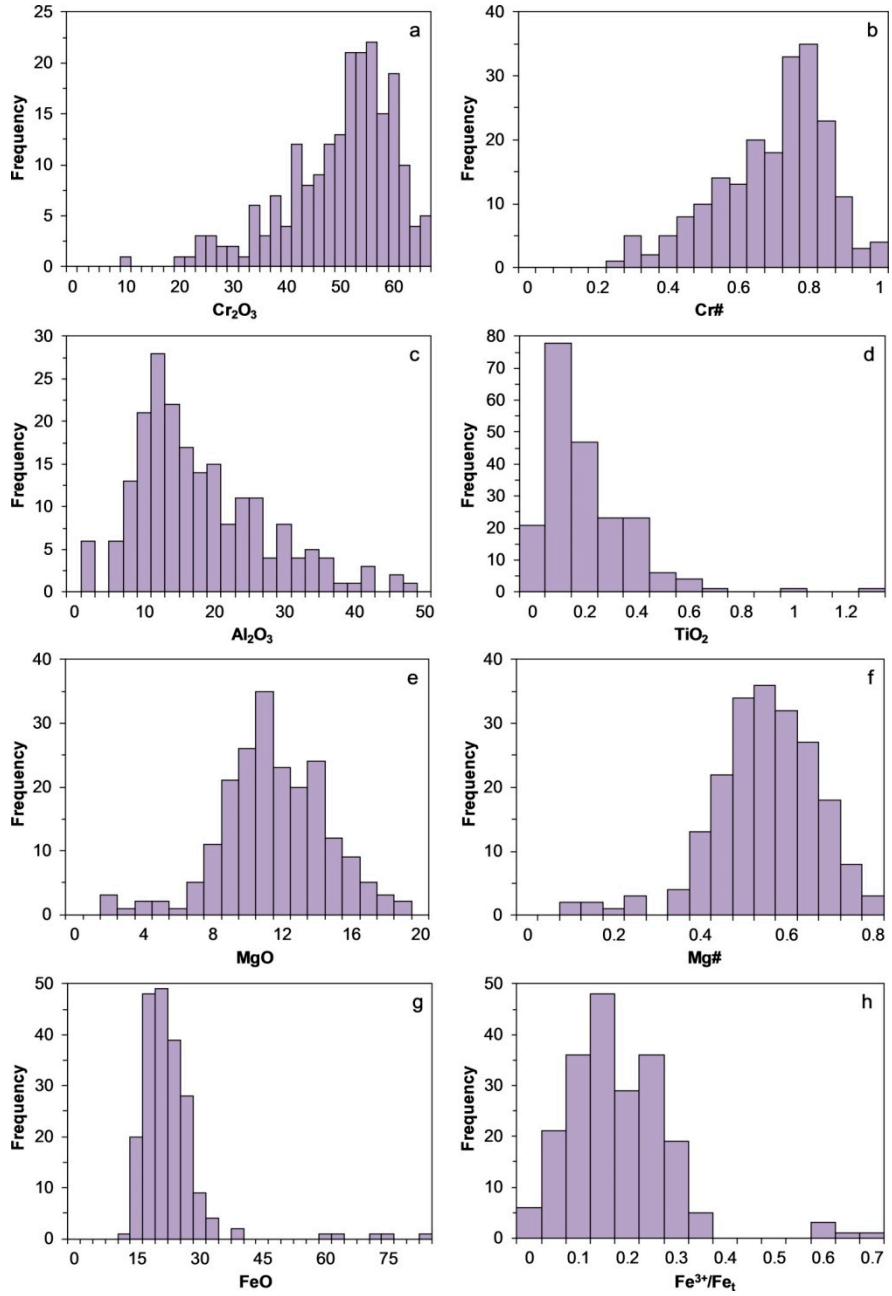

Figure 8. Histograms of the frequency distribution of the major components in chromspinels from the Sabantuy paleoplacer: (**a**) Cr_2O_3, (**b**) Cr# = Cr/(Cr + Al), (**c**) Al_2O_3, (**d**) TiO_2, (**e**) MgO, (**f**) Mg# = Mg/(Mg + Fe^{2+}), (**g**) FeO, (**h**) Fe^{3+}/Fe_t. Note: $Fe_t = Fe^{2+} + Fe^{3+}$.

Almost all studied chromspinels occur along the Cr–Al side of the triangle diagram $Cr–^{3+}Al–^{3+}–Fe^{3+}$, which reflects the critical role of the chromium–aluminum substitution typical for chromites from ophiolite peridotites and mid-ocean ridge basalts (MORB) (Figure 9) [3,4,42]. The amount of trivalent iron is minor, which corresponds to the low value of the iron oxidation coefficient $Fe^{3+}/Fe_t < 0.2$. Chromspinels of the Sabantuy paleoplacer are characterized by a direct correlation between Mg# and Cr# (Figure 10). The major part of the selection occurs in the field of island-arc peridotites, partly overlapping with fields of chromspinels of other genetic types.

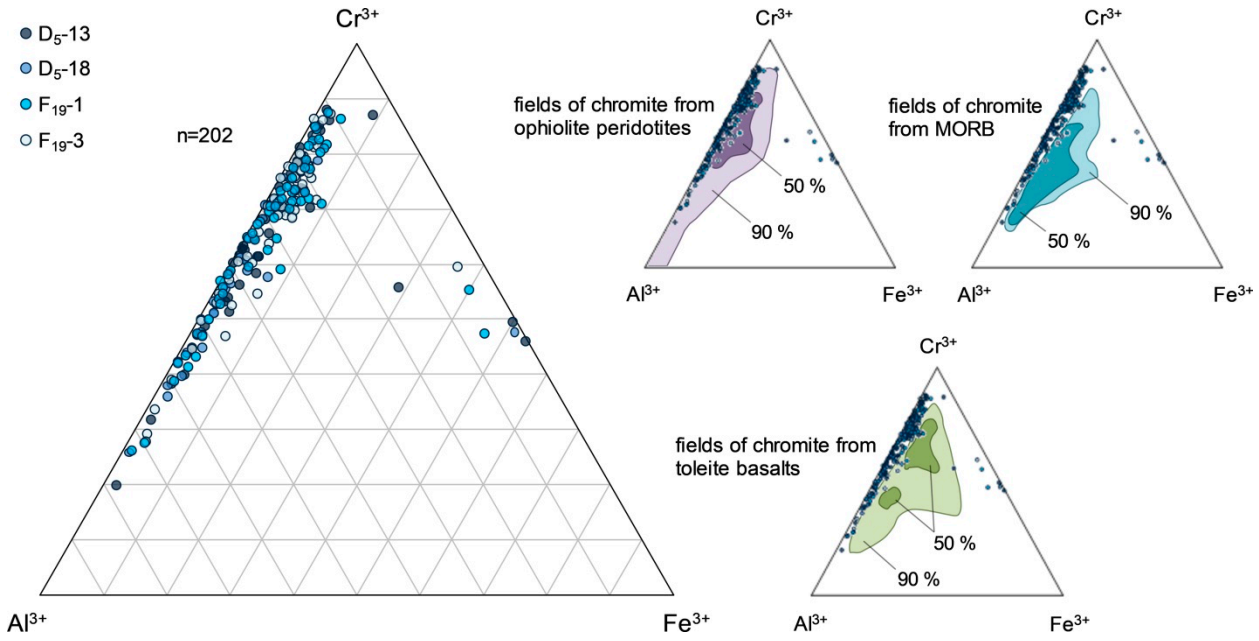

Figure 9. Ternary Cr^{3+}–Al^{3+}–Fe^{3+} diagrams for chromspinels from the Sabantuy paleoplacer in comparison with fields of chromspinel composition from different complexes taken from [42].

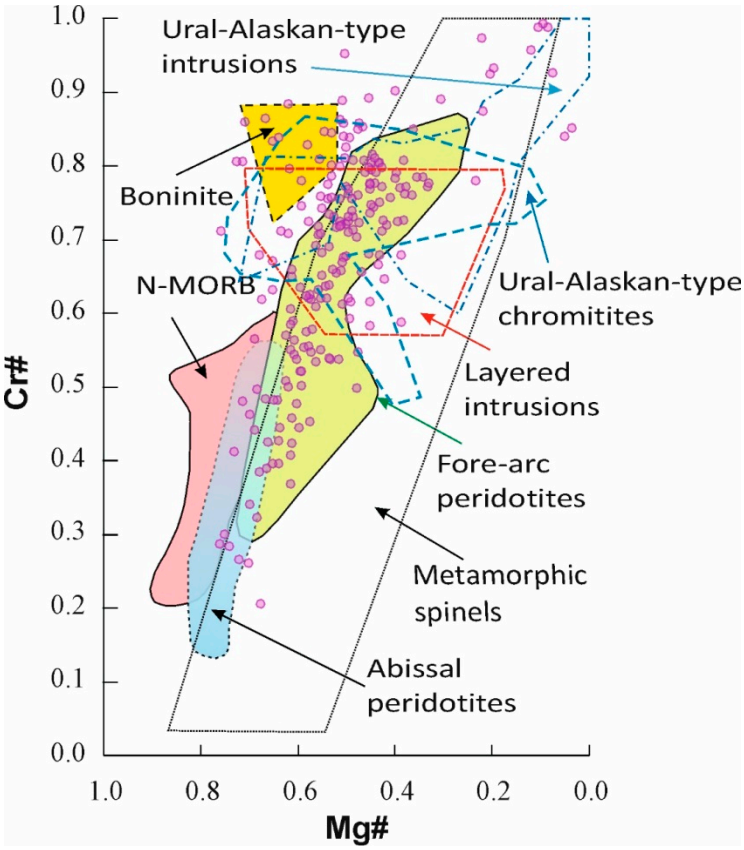

Figure 10. Diagram Mg#–Cr# for chromspinel from Sabantuy paleoplacer. Fields for chromspinel in abyssal peridotites, boninite, N-MORB and layered intrusions were taken from [3]; fields for Alaskan-type intrusions were taken from [42]; fields for Ural-Alaskan-type chromitites were taken from [34]; fields for fore-arc peridotites were taken from [43]; the field for metamorphic spinel was taken from [44].

4.5. Inclusions in Chromspinels

Overlapping compositions of chromspinel from the Sabantuy paleoplacer with the fields of chromspinels of different nature (Figure 10) do not allow suggesting a certain source for detrital chromites. Inclusions in chromspinel may carry important information about the protolith nature [13,45]. Investigation of about 1000 grains of chromite from the Sabantuy paleoplacer under reflected light microscope allow to reveal inclusions in 24 grains, as follows: (1) solid-state monomineralic, (2) polymineralic of unclear nature and (3) melt inclusions. Most of these inclusions were studied using SEM and X-ray microprobe (see Section 2. Materials and Methods). The size of inclusions varies from 1–5 to 50–100 μm. Fine inclusions less than 10 μm were only studied on SEM with an EDS spectrometer.

No inclusions of platinum-group minerals were found. Olivine inclusions were identified in five chromite grains. Clinopyroxene was found in four grains, and orthopyroxene was found in eight grains. Amphibole is the best widespread mineral in inclusions, and it was recognized in 14 chromite grains. Only one grain of chromspinel (grain 5–26 sample D_5-13) contained inclusions of olivine, orthopyroxene and amphibole at once. No coexisting inclusions of olivine and clinopyroxene were detected. Three chromspinel grains contained partly recrystallized melt inclusions. Coexisting clinopyroxene and amphibole were revealed in melt and polymineralic inclusions. In addition, single inclusions of iron, copper and nickel sulphides were found in chromspinel, but their small size does not allow to obtain high-quality data and identifying their mineral type. Ca-carbonate inclusions were recorded in two chromspinel grains. In most cases, the inclusions were safely encapsulated in chromite and well-preserved. However, some of them were partly or completely replaced by secondary low-temperature minerals.

Olivine is always presented as monomineralic inclusions with the size ranging from 6 to 90 μm along the long axis (Figure 11). Single inclusions in chromspinel are common, but one grain showed an abundant dissemination of fine olivine grains (Figure 11f). The shape of inclusions is elongated, rounded or short-prismatic. All olivine is represented by forsterite with Mg# = 0.93–0.95 (Table 3). According to Garuti and coauthors [34], olivine inclusions in ore-forming chromspinel of the Uralian ophiolite complexes usually show high MgO content and Mg# = 0.95–0.97. The NiO content in olivines varies from 0.35 to 0.60 wt.%, which is compatible with compositions of forsterite from mantle peridotites in the Urals [34,46]. The admixture of calcium and manganese is minor and close to the detection limits of electron probe microanalyses. Such a feature of olivine is also typical for ophiolite peridotites. All of the studied olivines were characterized by an extremely high Cr_2O_3 content ranging from 0.4 to 2 wt.%. We suggest that it is caused by an interference of chromium during the X-ray microprobe analysis of fine olivine inclusions in chromspinel. This phenomenon was not checked using the ZAF correction procedure; therefore, the chromium content in olivine is not discussed below. The correlation of Mg# in olivine from inclusions and Cr# in host chromspinel indicates that all points are distributed along the left side of the OSMA field (Figure 12). The shift of olivine to a more high-Mg# composition area is probably explained by the re-equilibration reaction between chromite and olivine noted in peridotites and chromitites [47].

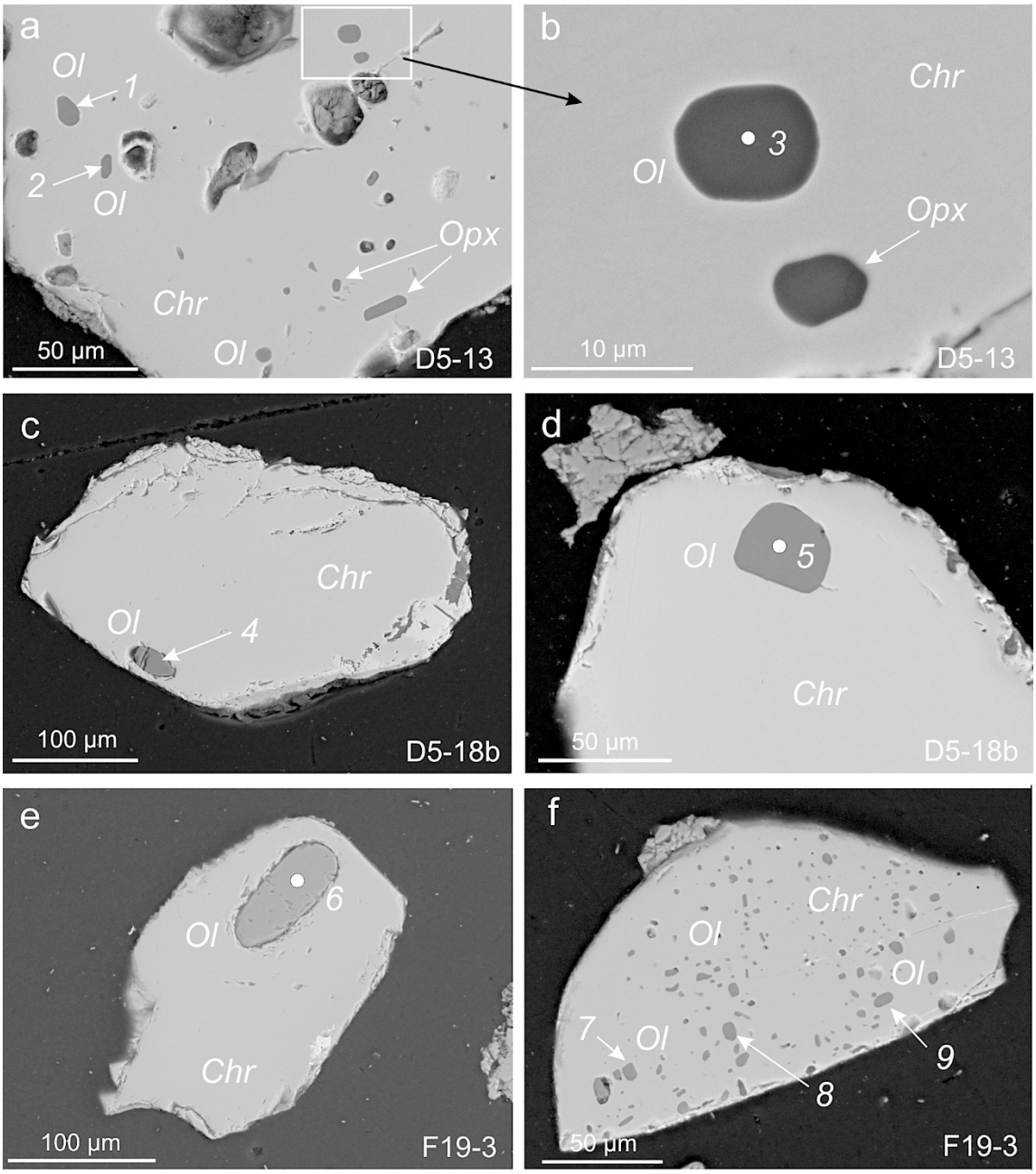

Figure 11. BSE images of monomineralic olivine (Ol) and orthopyroxene (Opx) inclusions in chromspinels (Chr) from the Sabantuy paleoplacer (samples D_5-13, D_5-18b, F_{19}-3): (**a**) numerous chromspinel-hosted olivine and orthopyroxene inclusions, (**b**) olivine and orthopyroxene inclusions, enlarged area of figure (**a**), (**c**,**d**) olivine inclusions, (**e**) rounded olivine inclusion, (**f**) abundant olivine inclusions in chromspinel. Note: the numbers indicate the points of the compositions presented in Table 3.

Table 3. The composition of olivine inclusions in chromite (wt.%).

Sample	D_5-13			D_5-18b			F_{19}-3		
Analytical Points	**1**	**2**	**3 ***	**4**	**5**	**6**	**7 ***	**8 ***	**9 ***
SiO_2	41.43	41.49	41.18	42.02	41.82	41.33	40.93	41.19	41
Cr_2O_3	1.20	1.23	2.00	0.72	0.67	0.35	1.52	1.20	1.64
FeO	6.72	6.27	6.31	5.88	6.93	7.14	6.5	6.42	6.54
MnO	0.09	0.07	n.d.	0.08	0.08	0.09	n.d.	n.d.	n.d.
MgO	51.34	51.70	50.17	50.85	50.77	51.14	50.61	50.70	50.19
CaO	n.d.	0.02	n.d.	n.d.	n.d.	n.d.	n.d.	n.d.	n.d.
NiO	0.47	0.43	0.34	0.38	0.49	0.53	0.44	0.49	0.64
Total	101.26	101.21	100.00	99.94	100.77	100.59	100.00	100.00	100.00
Mg/(Mg + Fe)	0.93	0.94	0.94	0.94	0.93	0.93	0.93	0.93	0.93
Cr#	0.54	0.54	0.54	0.75	0.61	0.39	0.52	0.52	0.52

*—analyses have been done using the SEM Jeol 6390 LV with EDS Oxford spectrometer and normalized to 100 wt.%. Cr# = Cr/(Cr + Al) in chromite host. n.d.—element is not detected. Analytical points (Figure 11).

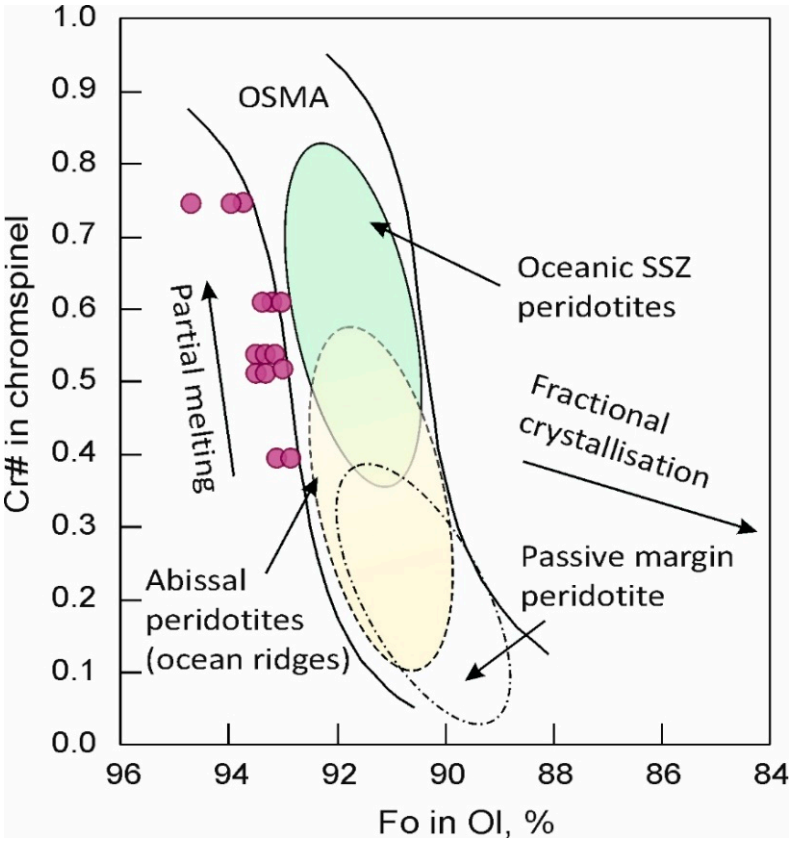

Figure 12. Compositional relationships between Fo content in olivine and Cr# in chromspinel from Sabantuy chromite paleoplacer. The olivine–spinel mantle array (OSMA) is after Arai [4,48]. SSZ—supra-subduction zone peridotites.

Clinopyroxene was found and studied in four grains of chromspinel. Clinopyroxene forms rounded monomineralic inclusions with the size of 30–70 μm (Figure 13a,b). However, it mainly occurs in polymineralic inclusions, some of which could be interpreted as recrystallized melt inclusions (Figure 13c,d). The size of these clinopyroxene crystals is commonly <20 μm. Clinopyroxene from monomineralic inclusions is high in magnesium number Mg# = 0.93–0.98, extremely low in alumina (Al_2O_3 < 1 wt.%) and high in Cr_2O_3 = 0.6–2 wt.% (Table 4), which is common for clinopyroxenes from chromitites of

ophiolite complexes [34,46]. Clinopyroxene of the solid-state inclusion from the sample F_{19}-3 shows 0.4–0.5 wt.% of Na_2O (Table 3). High-alumina clinopyroxene (fassaite) with up to 1.5 wt.% TiO_2 was detected in the composition of polymineralic inclusions with amphibole (Table 4). Except for pyroxene and amphibole, such inclusions contain Na-rich and Ca-rich plagioclase (Figure 13d). Clinopyroxene in another inclusion (without plagioclase) corresponds to high-magnesian Cr-diopside of the peridotite type [29,34,46].

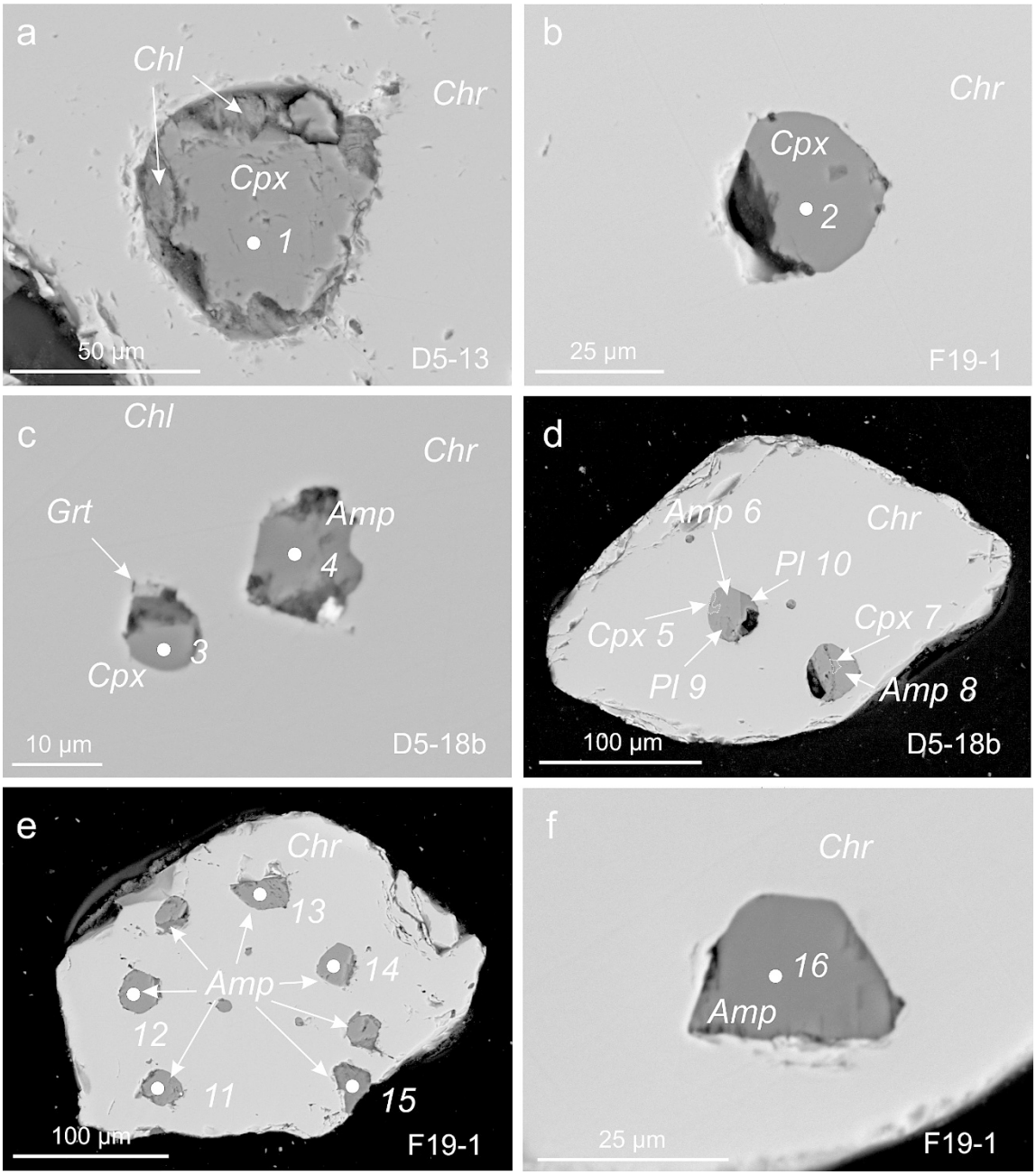

Figure 13. BSE images of monomineralic and polymineralic clinopyroxene (Cpx) and amphibole (Amp) inclusions in chromspinels (Chr) from the Sabantuy paleoplacer (samples D_5-13, D_5-18b, F_{19}-1): (**a**,**b**) clinopyroxene inclusions partially replaced by chlorite (Chl); (**c**,**d**) polymineralic inclusions in chromite. Grt—Ca-rich garnet; (**e**) abundant amphibole inclusions in chromite; (**f**) single amphibole inclusion. Note: the numbers indicate the points of the compositions presented in Table 4.

Table 4. The composition of monomineralic and polymineralic clinopyroxene–amphibole–plagioclase inclusions in chromite (wt.%).

Sample	D_5-13	F_{19}-3	D_5-18b					
Analytical Points	**1**	**2**	**3 ***	**4 ***	**5 ***	**6 ***	**7 ***	**8 ***
SiO_2	54.04	54.50	53.53	43.44	46.18	49.07	53.83	48.13
TiO_2	0.07	0.08	0.00	0.6	1.49	1.59	0.35	2.15
Al_2O_3	1.03	0.86	1.37	13.85	12.06	9.77	1.74	9.62
Cr_2O_3	1.05	2.05	1.75	3.21	1.03	2.88	1.83	2.88
FeO	2.24	1.93	1.90	3.29	4.80	3.47	2.34	3.52
MnO	0.06	0.05	n.d.	n.d.	n.d.	n.d.	n.d.	n.d.
MgO	17.41	16.80	16.67	18.75	11.37	19.07	16.90	18.61
CaO	24.35	23.79	24.78	13.11	23.08	12.38	23.01	12.61
Na_2O	0.19	0.54	0.00	3.46	n.d.	1.76	0.00	2.30
K_2O	n.d.	n.d.	n.d.	0.28	n.d.	n.d.	n.d.	0.18
Total	100.44	100.60	100.00	100.00	100.00	100.00	100.00	100.00
Mg/(Mg + Fe)	0.93	0.94	0.94	0.91	0.81	0.91	0.93	0.91
Sample	**D_5-18b**		**F_{19}-1**					
Analytical Points	**9***	**10 ***	**11**	**12**	**13**	**14**	**15**	**16**
SiO_2	47.37	68.79	49.74	49.40	49.43	49.38	49.17	52.13
TiO_2	n.d.	n.d.	0.28	0.34	0.23	0.36	0.26	0.04
Al_2O_3	32.93	18.66	7.65	7.40	7.47	7.53	7.61	5.82
Cr_2O_3	0.59	0.80	1.64	1.51	1.45	1.57	1.49	2.15
FeO	0.50	0.21	4.45	4.75	4.79	4.72	4.93	2.20
MnO	n.d.	n.d.	n.d.	0.05	0.07	0.05	0.06	0.09
MgO	n.d.	n.d.	19.63	19.32	19.47	19.39	19.87	21.81
CaO	16.89	0.89	12.92	12.78	12.93	12.84	12.92	12.36
Na_2O	1.73	10.65	1.20	1.18	1.14	1.16	1.08	1.58
K_2O	n.d.	n.d.	0.44	0.53	0.51	0.49	0.60	0.05
Total	100.00	100	97.95	97.26	97.49	97.49	97.99	98.23
Mg/(Mg + Fe)			0.89	0.88	0.88	0.88	0.88	0.95

Note: 1, 2, 3, 5, 7—clinopyroxene, 4, 6, 8, 11–16—amphibole. 9, 10—plagioclase. *—analyses have been conducted using the SEM Jeol 6390 LV with EDS Oxford spectrometer and normalized to 100 wt.%. n.d.—element is not detected. Analytical points (Figure 13).

Orthopyroxene was detected as monomineralic inclusions in eight chromite grains, and in one grain, it coexists with inclusions of olivine (Figures 11a and 14). Orthopyroxene forms prismatic crystals with the size of a few microns to 60 μm (Figure 14). All of the studied orthopyroxenes are highly magnesian, Mg# = 0.91–0.94 (Table 5). The Al_2O_3 content varies from 0.3 to 1.8 wt.%, and the CaO content ranges from 0.4 to 1 wt.%. The Cr_2O_3 content is typically high (0.9–1.3 wt.%), such as in clinopyroxene. The composition of orthopyroxene from inclusions is compatible with that of the Uralian peridotites [29,34,46].

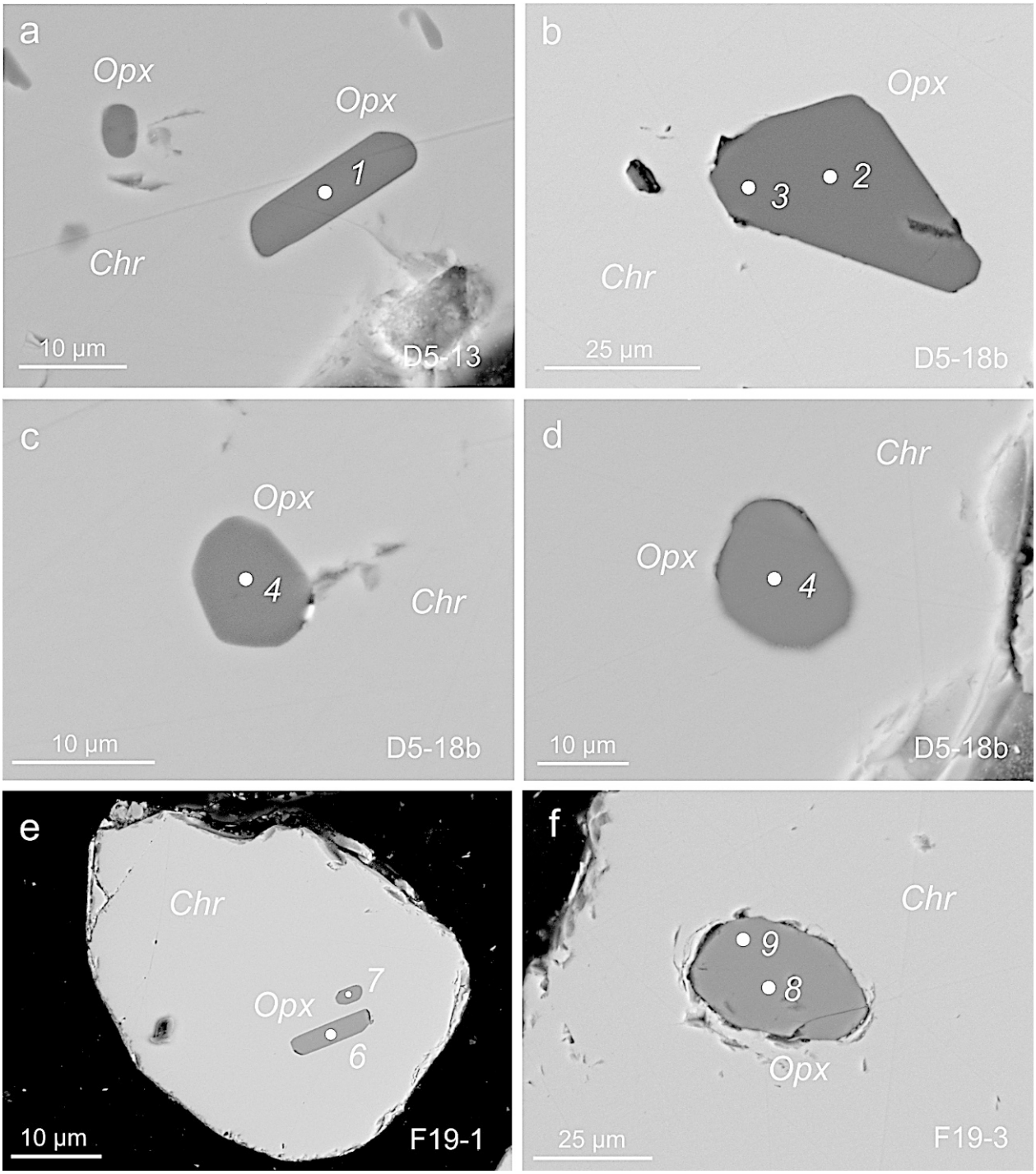

Figure 14. BSE images of monomineralic orthopyroxene (Opx) inclusions in chromspinels (Chr) from the Sabantuy paleoplacer (samples D_5-13, D_5-18b, F_{19}-1, F_{19}-3): (**a**,**b**) prismatic orthopyroxene inclusions, (**c**,**d**) small sub-rounded orthopyroxene inclusions, (**e**) prismatic orthopyroxene inclusions, (**f**) sub-angular orthopyroxene inclusion. Note: the numbers indicate the points of the compositions presented in Table 5.

Table 5. The composition of monomineral orthopyroxene inclusions in chromite (wt.%).

Sample	D_5-13	D_5-18				F_{19}-1		F_{19}-3	
Analytical Points	**1 ***	**2**	**3**	**4 ***	**5 ***	**6**	**7**	**8**	**9**
SiO_2	56.22	58.12	58.41	57.19	56.98	57.06	57.32	56.31	57.11
TiO_2	n.d.	0.04	n.d.	n.d.	n.d.	n.d.	n.d.	n.d.	n.d.
Al_2O_3	1.60	0.36	0.35	1.25	1.19	1.31	1.26	1.80	1.77
Cr_2O_3	1.78	0.97	1.07	1.39	0.92	1.27	1.19	1.06	0.93
FeO	5.94	4.56	4.42	4.49	5.66	4.45	4.33	5.72	5.80
MnO	n.d.	0.09	0.09	n.d.	0.23	0.16	0.15	0.11	0.16
MgO	34.00	36.52	36.15	35.17	34.83	35.06	35.18	34.40	34.32
CaO	0.45	0.41	0.47	0.52	0.19	0.97	0.94	0.81	0.82
Total	100.00	101.17	101.02	100.00	100.00	100.36	100.48	100.32	101.00
Mg/(Mg + Fe)	0.91	0.94	0.94	0.93	0.92	0.93	0.94	0.92	0.91

Note: *—analyses have been conducted using the SEM Jeol 6390 LV with EDS Oxford spectrometer and normalized to 100 wt.%. n.d.—element is not detected. Analytical points (Figure 14).

Amphibole occurs in inclusions more often than other minerals. It was found in 14 grains of chromspinel both as solid-state monomineral inclusions (Figure 13e,f) and in polymineralic aggregates (Figure 13c,d), in particular, in recrystallized melt inclusions (Figure 13b–d). The size of amphibole grains ranges from several microns to 50–60 μm. In the grain (13–17) represented by iron-rich chromspinel with TiO_2 = 0.8 wt.%, inclusions of amphibole occur radially in the center of the grain, presumably, along the growth zones of chromspinel (Figure 13e). The composition of amphibole in inclusions varies widely, i.e., Mg# ranges from 0.96 to 0.5, Al_2O_3 from 4 to 19 wt.% and TiO_2 from 0 to 2 wt.% (Table 4). It commonly contains a significant amount of K_2O>0.4 wt.%. Most of the high-Mg# amphiboles from polymineralic and monomineralic inclusions show Al_2O_3 < 10 wt.% and low values of TiO_2 (<1 wt.%), which reflects their relatively low-temperature origin [49]. Amphiboles from melt inclusions typically have Mg# < 0.80, Al_2O_3 > 10 wt.% and TiO_2 > 1 wt.%, which indicates their high-temperature origin [49].

Recrystallized melt inclusions were discovered in three chromspinel grains (3–2, 8–49, 15–30). They have a rounded shape and a size from a few to 20 μm (Figure 15). Their host grains of chromite have Cr# < 0.47, TiO_2 > 0.5 wt.% and Mg# = 0.46, 0.47 and 0.74, respectively (Table 2). Melt inclusions contain an aggregate of prismatic and needle-shaped crystals of amphibole and clinopyroxene. Interstices between them are filled with micrograins of plagioclase and an isotropic matter, which is presumably glass with empty holes (fluid bubbles). Such structures reflect chilled conditions of crystallization. It is difficult to identify the true chemical composition of minerals due to the small sizes of microlites. The composition of glass was measured in two inclusions from different chromspinel grains. It is compatible with the composition of high-Al andesibasalts and andesite (Table 6). The bulk composition of two melt inclusions measured by the area (SEM facilities) is close to mid-ocean ridge basalts. These estimates are rather approximate since the inclusions are high in Cr_2O_3 due to the contribution of host chromite. Thus, the bulk composition of the inclusions should be given some extra corrections.

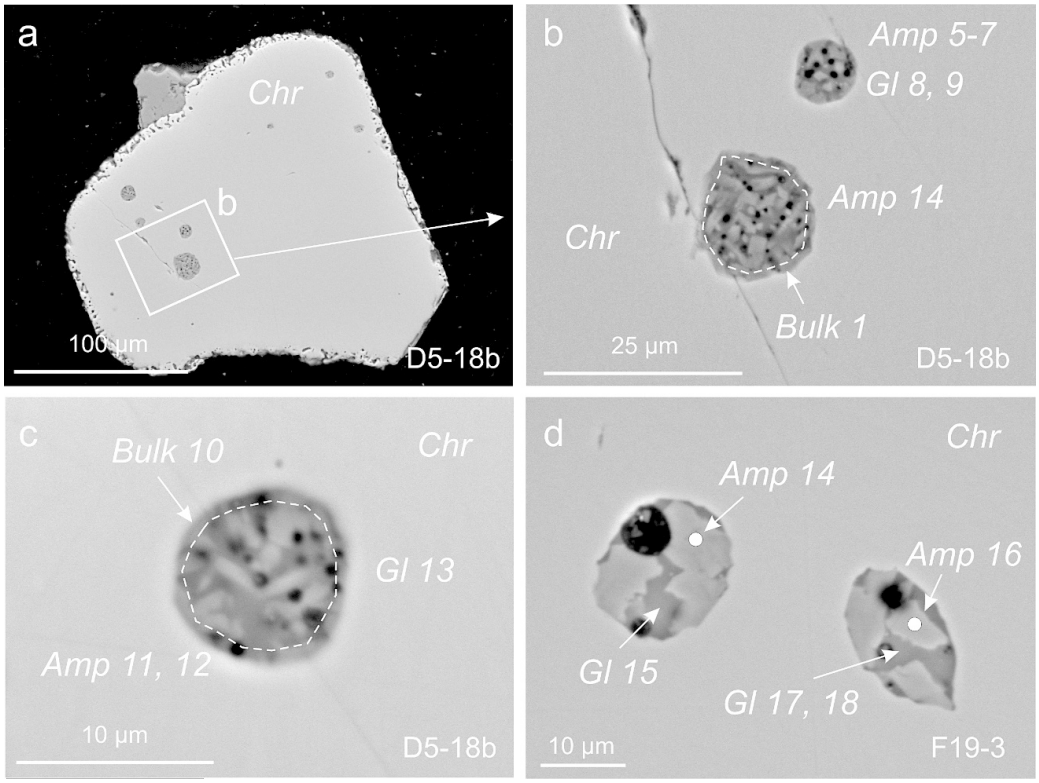

Figure 15. BSE images of melt inclusions in chromites (Chr) from the Sabantuy paleoplacer (samples D_5-18b, F_{19}-3): (**a**) numerous recrystallized melt inclusions in chromite, (**b**) enlarged area of figure (**a**), (**c**,**d**) recrystallized melt inclusions. Amp—amphibole, Gl—glass, Bulk—area, where the bulk composition of melt inclusions was determined. Note: the numbers indicate the points of the compositions presented in Table 6.

Table 6. The bulk composition of melt inclusions, glass and constituent amphiboles (wt.%).

Sample			**D_5-18b**				**D_5-18b**		
Analytical Points	**1**	**2**	**3**	**4**	**5**	**6**	**7**	**8**	**9**
SiO_2	46.7	48.1	48.4	47.1	42.1	44.4	45.1	49.5	43.9
TiO_2	1.3	1.7	1.5	0.9	1.3	1.4	1.4	1.3	1.0
Al_2O_3	17.6	13.9	15.0	18.8	15.4	17.0	16.9	19.4	20.9
Cr_2O_3	4.9	1.8	1.6	7.7	8.1	5.0	4.7	5.2	8.2
FeO	8.6	7.4	8.0	8.3	8.7	8.5	8.5	7.2	8.1
MnO	n.d.	n.d.	n.d.	n.d.	n.d.	n.d.	0.3	0.0	0.0
MgO	8.1	13.2	11.1	5.2	11.7	10.1	10.5	4.7	6.7
CaO	10.5	13.0	13.2	8.3	11.8	11.8	10.9	9.0	8.4
Na_2O	2.2	1.0	1.1	3.7	1.0	1.8	1.3	3.3	2.7
K_2O	n.d.	n.d.	n.d.	n.d.	n.d.	n.d.	n.d.	0.2	0.2
Total	100.0	100.0	100.0	100.0	100.0	100.0	100.0	100.0	100.0
Mg/(Mg + Fe)	0.6	0.8	0.7	0.5	0.7	0.7	0.7	0.5	0.6
Sample			**D_5-18b**				**F_{19}-3**		
Analytical Points	**10**	**11**	**12**	**13**	**14**	**15**	**16**	**17**	**18**
SiO_2	51.3	48.9	50.4	53.1	46.1	55.4	48.0	54.7	56.4
TiO_2	1.5	1.5	1.5	1.1	2.1	1.2	1.9	1.7	1.0
Al_2O_3	18.4	16.1	17.4	20.1	11.9	22.5	9.7	21.3	21.9
Cr_2O_3	1.7	1.5	1.2	1.9	0.8	0.9	0.9	1.3	1.0
FeO	7.4	7.6	7.6	6.1	7.8	6.1	6.9	6.9	6.5
MnO	n.d.	n.d.	n.d.	n.d.	0.2	n.d.	n.d.	n.d.	n.d.
MgO	5.6	9.8	7.5	3.9	14.5	1.2	18.3	0.5	0.5
CaO	11.7	12.8	12.7	10.2	16.5	6.9	14.4	7.9	8.7
Na_2O	2.2	1.2	1.5	3.0	0.0	5.9	0.0	5.2	4.7
K_2O	0.3	0.2	0.2	0.3	n.d.	n.d.	n.d.	n.d.	n.d.
Total	100.0	100.0	100.0	100.0	100.0	100.0	100.0	100.0	100.0
Mg/(Mg + Fe)	0.6	0.7	0.6	0.5	0.8	0.3	0.8	0.1	0.1

Note: 1, 10—bulk composition of melt inclusion, 2, 3, 5–7, 11, 12, 14, 16—amphibole, 4, 8, 9, 13, 15, 17, 18—glass. All analyses have been conducted using the SEM Jeol 6390 LV with EDS Oxford spectrometer and normalized to 100 wt.%. n.d.—element is not detected. Analytical points (Figure 15).

Along with the above minerals, chromspinels contain inclusions of Ca-carbonate, sulphides of nickel, iron and copper that require further research and are not considered in the current paper.

5. Discussion

5.1. Potential Sources of Deposits

The petrographic study of sandstones of the Sabantuy chromite paleoplacer shows that the main contributors in their composition were metamorphic and sedimentary complexes. Varied roundness of compositionally similar fragments suggests that the time and conditions of their transfer and sedimentation are also different. The Uralian orogenic belt was the main supply region of terrigenous material for these sedimentary basins during the whole Permian time [6,7,22]. As it was established, the Ural Foredeep starts to form in the Early Permian and by the dawn of the Biarmian (Guadalupian) epoch, it had completely filled and detrital material was distributed further westwards, increasing the thickness of the sedimentary cover of the East European Platform (Figure 16). Mizens and Maslov conducted lithological and geochemical studies of sandstones of the molasse formation in the southern part of the Ural Foredeep, which rocks of the Kazanian Stage are also attributed to [6]. U-Pb isotope dating of detrital zircons from molasse sandstones yields the Proterozoic age for most zircon populations and the Early Paleozoic age for their minor part [6]. Thus, the Riphean sedimentary and metamorphic complexes of the Bashkirian Meganticlinorium are considered the main supplier of detrital material for the studied sandstones [22].

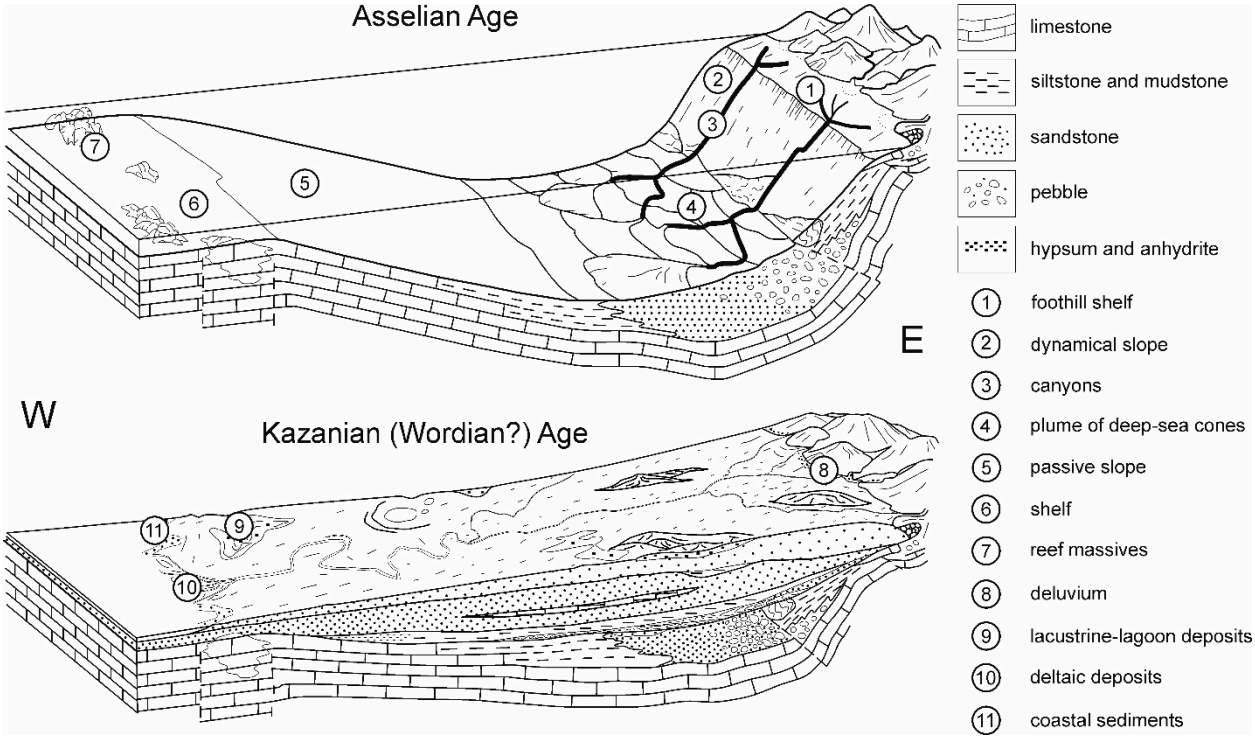

Figure 16. A simplified cross-section of the Ural Foredeep for the Early Permian (**top**) and Middle Permian time (**bottom**), modified after Mizens [50].

The appearance of the chromite-bearing horizon in the studied section of Kazanian sediments marks an exhumation and erosion of chromite-bearing complexes in the supply region. Notably, the boundary between the chromite-bearing horizon and underlying sandstones is rather abrupt. The amount of chromspinel in underlying rocks is not higher than 1 wt.%, whereas it is up to 30 wt.% in chromitolite bed and 10–15 wt.% in sandstones

overlying the ore horizon. No one object with an economically important content of detrital chromspinel, such as the Sabantuy paleoplacer, had been ever known in the Ural Foredeep before [36]. It was formerly suggested that detrital chromites in the Permian sediments of the Southern Pre-Urals were derived from oceanic and suprasubduction mafic–ultramafic complexes of Uralides [6].

The noted class of chromspinel grain size (0.15–0.25 mm) is typical of placers [17,51,52]. Grains with this size and a density of ca. 4–5 g/cm^3 seem to be the most transportable and transferred for a relatively long distance. Transportation of bigger grains is hardly possible; therefore, we believe that sources for the Sabantuy paleoplacer were quite remote, probably 100–200 km far from the placer. Such provenance could be ophiolite complexes of the Main Uralian Fault (MUF) zone and associated serpentinite mélange and volcanic rocks, as well as peridotite allochthones, tectonically moved westwards from MUF through the Ural-Tau dome structures [29,34,46,53]. For example, the Kraka ultramafic massif, being the largest peridotite allochtone (more than 900 sq. km of area) in the Southern Urals, is the nearest ultramafic body to the Sabantuy placer (Figure 1b). Island-arc volcanic complexes of Paleozoic age in the Magnitogorsk zone (Figure 1b), situated to the east of MUF, could be an additional source for chromspinel [54–56].

The results of the geological survey indicate that within 100 km from the Sabantuy ore occurrence, there are no mafic–ultramafic or volcanic complexes that could be considered sources for chromspinel [37]. The ore material was apparently concentrated in the Sabantuy paleoplacer due to intermediate collectors since a long direct transfer without precipitation of heavy minerals is hardly possible.

The study of lithology and petrography of sedimentary rocks in the Sabantuy paleoplacer revealed that olivine and orthopyroxene are absent among clastic minerals, whereas they are major for ophiolite peridotites. It is probably related to olivine and orthopyroxene's less resistance in the weathering crust and exogenic environment in comparison with chromite [57]. Clinopyroxene occurs as rare grains. Among them, augite, omphacite and diopside were identified. Only diopside is compositionally closest to clinopyroxene from ophiolite peridotites and inclusions in the Sabantuy chromites, and it can be a product of peridotite erosion. Besides, sandstones contain single fragments of serpentinites and debris of mineral grains (in order of decreasing amount): feldspar, serpentine, chlorite, amphibole, scapolite, biotite, garnet, epidote and tourmaline.

The bulk composition of studied melt inclusions in several chromspinel grains corresponds to basalt and andesite. Similar compositions have an interstitial glass preserved in some melt inclusions. This fact clearly indicates that volcanic rocks were one of the sources of detrital chromspinel. The dendritic architecture of facets in some chromite crystals (Figure 6c,f) gives another piece of evidence for the volcanic origin of chromspinel [58].

All these data testify the heterogeneous sources of sandy rocks and chromspinel in particular and, possibly, quite a remote transfer of chromspinel from supply regions to the placer.

5.2. Potential Sources for Chromspinels

Chromspinels are reliable petrological indicators of P-T-fO_2 conditions, geotectonic settings and composition of host rocks. They are widely applied for petrogenetic and tectonic reconstructions [1–4,45,48,59]. Our research showed that chromspinel of the Sabantuy paleoplacer had broad variations ruled by substitution of trivalent Al^{3+} and Cr^{3+} and bivalent Fe^{2+} and Mg cations. The range of these variations is clearly displayed on the Cr#–Mg# diagram (Figure 10). The diagram shows fields of chromspinels from peridotites of different geotectonic settings, layered intrusions, Uralian-Alaskan-type intrusion and chromitites, MORB basalts, boninites and metamorphic complexes. Most fields have significant overlap areas, whereas compositions of the studied chromspinels are also distributed along several fields at once, which does not allow suggesting a single source for chromites.

The results of the compositional analysis of monomineralic, polymineralic and melt inclusions (Section 4.5) indicate that chromites could have a volcanogenic origin in addition to their presumed peridotite source. However, since inclusions in chromites are rare, it is impossible to get a general statistic view and define the main type of rocks that supplied chromites to the Sabantuy paleoplacer. To solve this problem, we can consider histograms of the distribution of different components in the studied chromites compared to typical objects (Figure 17). We used two components of chromspinel Al_2O_3 and Cr_2O_3 with the widest range of values for this purpose. For comparison, we chose peridotites of the Uralian ophiolite complexes without chromitites (778 analyses) [29,34,46,60,61], the Uralian ophiolites with chromite ore (1954 analyses) [34,46], ophiolite complexes worldwide (5453 analyses) [42], island-arc volcanic rocks of the Magnitogorsk zone in the Southern Urals (142 analyses) ([54–56] and our unpublished data) and MORB basalts worldwide (296 analyses) [42].

As shown in Section 4.4., all histograms for chromspinel from the Sabantuy paleoplacer show a unimodal distribution of components with distinctly identify maximums (Figure 8). It allows defining the prevalent composition of chromspinel in the placer fairly confidently and comparing it with compositions of chromspinels from typical geological objects, which can be potential sources. It is clear that the distribution pattern for Al_2O_3 and Cr_2O_3 in the studied chromspinels with the maximums of 12 wt.% and 52–56 wt.%, respectively (Figure 17a), differs greatly from the distribution model for these components in island-arc volcanic rocks in the Southern Urals, where low-Al and extremely high-Cr chromites prevail dramatically, whereas chromites with the elevated alumina content are almost absent (Figure 17f). We reach a similar conclusion comparing the studied chromites with chromspinel from oceanic basalts, where far more high aluminum and fewer chromium compositions dominate (Figure 17e). The comparison with chromspinels from the Uralian ophiolite complexes excluding associated chromite ores shows an essential difference akin to that for oceanic basalts. The maximum of Al_2O_3 for peridotites is recorded at the level of 25–30 wt.%, the maximum of Cr_2O_3 is in the range of 40–45 wt.% (Figure 17b). The model of Al_2O_3 and Cr_2O_3 distribution in chromspinels of worldwide ophiolite complexes is essentially closer to the chromspinels we studied (Figure 17d). Thus, the statistical maximum of Al_2O_3 in worldwide ophiolites is registered in the interval of 10–20 wt.%, whereas the maximum of Cr_2O_3 is in the range of 40–45 wt.% (harzburgite-type chromites) with a significant amount of high-Cr chromites in the interval 50–60 wt.% of Cr_2O_3 in the histogram. It is specified based on a much more comprehensive sampling of chromite ores associated with ophiolites. This pattern is similar when we study the distribution of Al_2O_3 and Cr_2O_3 in the Uralian ophiolite complexes, taking into account the compositions of chromite ores (Figure 17c). In this case, histograms for the studied detrital chromites and ophiolites show comparable maximums in the interval of 10–12 wt.% Al_2O_3 and 50–60 wt.% Cr_2O_3, while less outstanding maximum typical of chromspinel from peridotites is preserved. This comparison fairly confidently suggests that peridotites of the Uralian ophiolite complexes and associated chromite ores were one of the main sources of chromspinel in the Sabantuy paleoplacer. The influence of ophiolite ore chromite and associated dunite can be prevalent in the Sabantuy paleoplacer, which explains the position of maximums in histograms of the Al_2O_3 and Cr_2O_3 distribution.

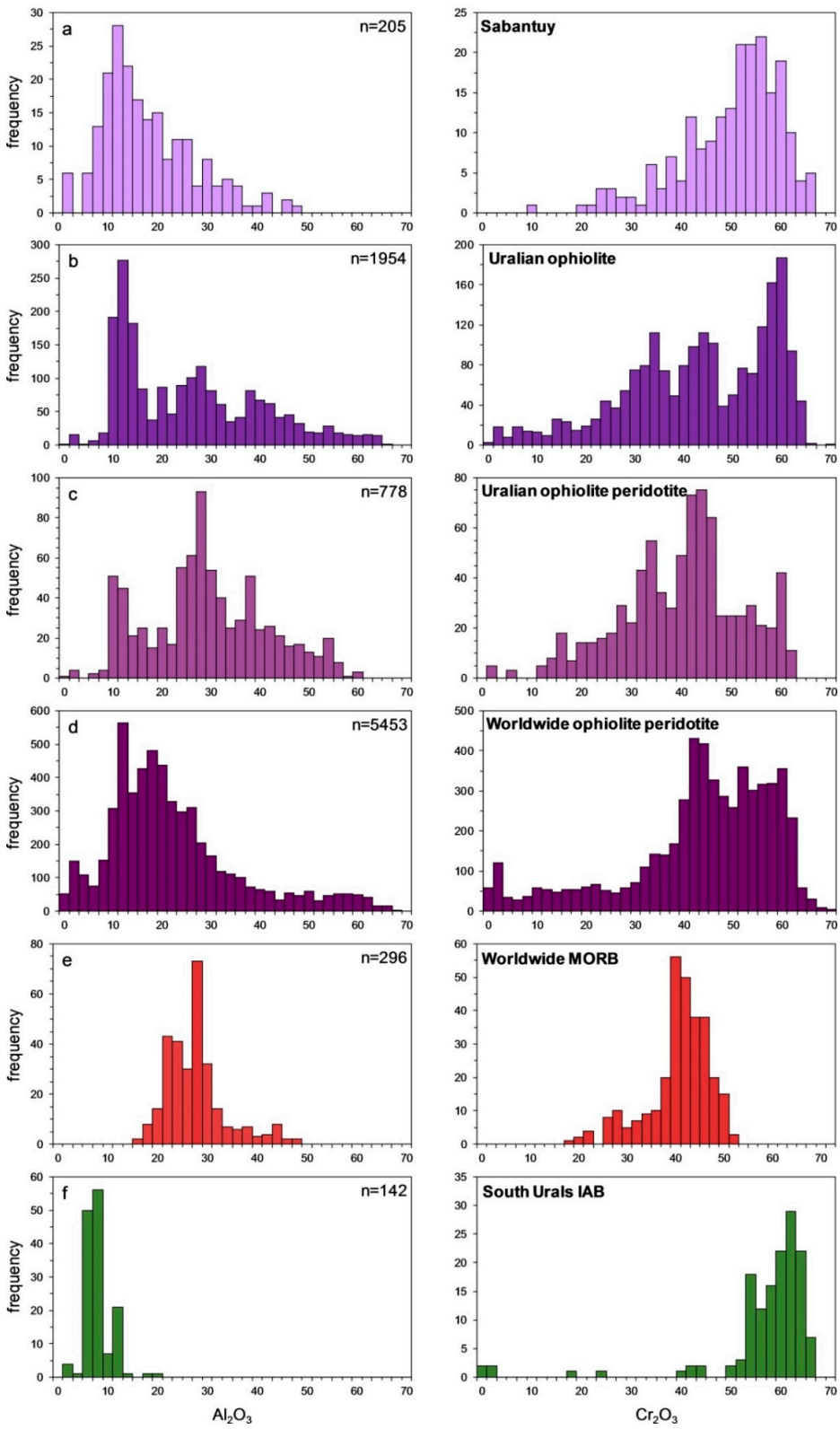

Figure 17. Histograms of Al_2O_3 and Cr_2O_3 frequency distribution for chromspinels from Sabantuy paleoplacer (**a**) (this study), Uralian ophiolite without chromitites (**b**) and ophiolite peridotite complexes, including chromite ores (**c**) [29,34,46,60,61], worldwide ophiolite complexes, including chromite ores (**d**) [42], MORB (**e**) [42] and Uralian island-arc basalts (**f**) ([53–56] and our unpublished data).

However, some issues have no rational explanation still. Thus, it is not clear why no one grain of high-Al chromspinel with Al_2O_3 > 50 wt.% was found among chromspinels of the Sabantuy paleoplacer, though it is typical of lherzolites widespread in the Main Uralian Fault zone in the Southern Urals and, in particular, in the largest Kraka peridotite allochthone closest to the Sabantuy placer [29,34,46]. Another intriguing fact is that sediments of placer contain almost no main rock-forming minerals of peridotites, i.e., olivine, orthopyroxene and clinopyroxene. Though we obtained some evidence that volcanic chromspinel participated in chromite placer, we do not know their provenance yet. It is possible, however, that they were derived from island-arc-related volcanic rocks of the Magnitogorsk zone.

We provided analyses using discrimination diagrams to define geotectonic settings, composition and facial conditions of protolith of rocks that were sources for detrital chromspinels. The TiO_2 content is one of the well-known indicators of the chromspinel origin, which is commonly used for dividing between peridotite and volcanic chromspinels and for identification volcanic rocks of different origin [11,16,45]. The TiO_2 content in the most studied chromspinels is less than 0.2 wt.%, and it corresponds to peridotite-type chromites. The TiO_2 content in chromites comprising melt inclusions is yet commonly higher than 0.4% and reaches 1.6%, which confirms their volcanic origin.

The Fe^{2+}/Fe^{3+} ratio is an additional criterion to divide chromspinels into the mantle and volcanic types [45,52]. Thus, chromite of mantle affinity usually has a high Fe^{2+}/Fe^{3+} ratio, and, vice versa, chromite from volcanic rocks has a low ratio. On the TiO_2–Fe^{2+}/Fe^{3+} diagram, most Sabantuy chromite falls into the peridotite field (Figure 18a). Chromspinel with a higher degree of oxidation state Fe^{2+}/Fe^{3+} < 5 corresponding to volcanic-type chromite is in a subordinate amount. However, an essential part of compositions lies in the uncertainty area, where the fields overlap.

Compositions of chromspinels matching to peridotites were plotted in the Mg#–Cr# diagram (Figure 18b). It shows that most figurative points overlap with the field of fore-arc peridotites, while the minor part overlaps with the field of abyssal peridotites. In the Al_2O_3–TiO_2 diagram (Figure 18c), almost all points are in the field of chromspinel from suprasubduction peridotites that commonly overlap with the field of oceanic peridotites. Provided that chromspinels with TiO_2 > 0.4% have a volcanic origin, which is validated by the presence of melt inclusions, the compositions in the Al_2O_3–TiO_2 diagram are distributed between island-arc and oceanic basalts with minor overlap area (Figure 18d). However, this conclusion is only probabilistic.

The presence of titanomagnetite with TiO_2 > 15 wt.% in the heavy fraction of the Sabantuy sediments indicates that clastic material could be also derived from ancient platform layered mafic–ultramafic intrusions or basalts, such as those known in the Archean and Proterozoic complexes of the Western Slope of the Urals and, in particular, in the Bashkirian Meganticlinorium [28].

The obtained data indicate that the most Sabantuy chromite could be derived from peridotites and chromitites of ophiolite complexes widespread in the Southern Urals, including huge peridotite allochthones transferred to the west from the Main Uralian Fault through the Ural-Tau anticline structures [22,29,34,46]. One such allochthon is the Kraka peridotite massif, hosting numerous chromite deposits of different scales [34,46]. In the modern coordinates, it is closest to the Sabantuy placer [38]. Mafic and ultramafic volcanic rocks of the oceanic and island-arc stage of the Urals development could be another source for chromites [53–56]. It cannot be excluded that ancient Archean and Proterozoic picrite and basalt dykes or layered mafic–ultramafic intrusions, widespread in the western slope of the Urals [22,28], contributed additional chromite in sedimentation basins in Permian time.

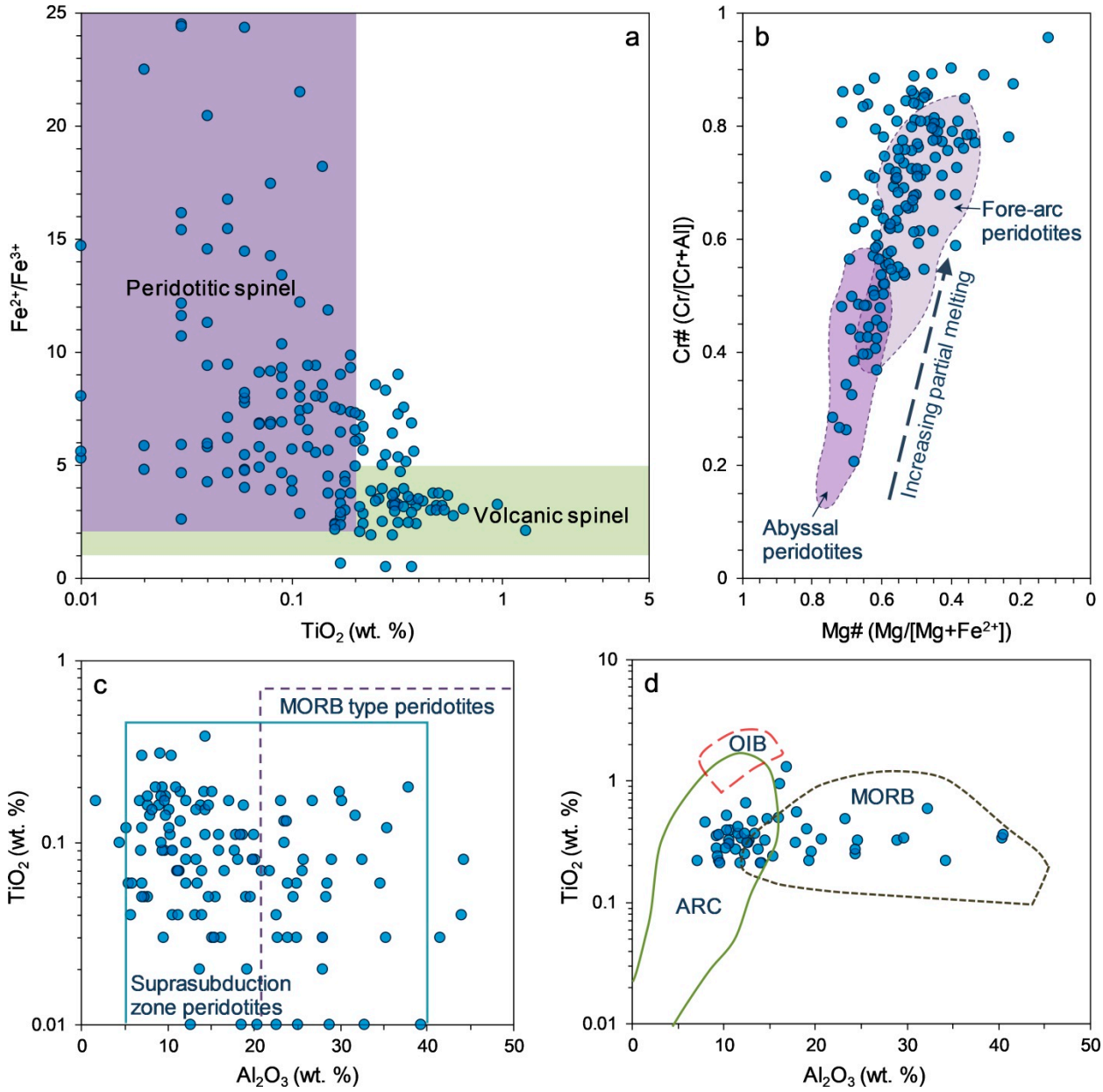

Figure 18. Discrimination diagrams for chromspinels of Sabantuy paleoplacer: (**a**) TiO_2 vs. Fe^{2+}/Fe^{3+} showing the compositions of all detrital chromspinels studied, peridotite and volcanic chromspinel fields are taken from [13]; (**b**) Mg# vs. Cr# for peridotite chromspinels, and fields are taken from [62]; (**c**) Al_2O_3 vs. TiO_2 for peridotite chromspinels, and fields are taken from [52]; (**d**) Al_2O_3 vs. TiO_2 for volcanic chromspinels, and fields are taken from [45]. MORB—middle ocean ridge basalts; ARC—island arc magmas; OIB—oceanic island basalt.

6. Conclusions

The Sabantuy chromite paleoplacer has been recently discovered in the Southern Pre-Urals region, at the eastern edge of the East European Platform in a transitional zone to the Ural Foredeep. The placer occurs in sandstones of the Kazanian stage of the Permian System. The ca. 1 m-thick chromite-bearing horizon is seated at a depth of 0.7–1.5 m. The chromite-rich sediments spread at least 300 m in meridional direction and over 50 m wide and occupy an area of about 15,000 sq.m. The actual distribution area of chromite-enriched rocks, as it seems, to exceed the above parameters and will be the next target for exploration and study. The structure of chromite-bearing sandstones is alternating of chromite-rich layers and layers with prevalent debris of rocks and silicate

minerals. Sandstone matrix is represented by Ca-carbonate. The heavy fraction in the sandstone reaches 70%. The content of chromspinel is 60–70% among ore minerals and up to 30–35% in bulk sandstone samples. The maximum Cr_2O_3 content in sandstone samples is 16–17 wt.%. Titanomagnetite, ilmenite, magnetite, ferropseudobrookite, hematite and rutile also present but in less amount than chromite. The prevalent size of chromspinel grains is 0.15–0.25 mm. It is mainly represented by whole subangular octahedral grains, rarely rounded-subrounded grains and debris. The composition of detrital chromspinel varies widely and is mostly constrained by the substitution of Al^{3+} and Cr^{3+}, Fe^{2+} and Mg^{2+} cations.

Most components of chromspinel show a unimodal statistical distribution that allows defining the prevalent chromite type in the placer. It complies with low-Al (Al_2O_3 = 12 wt.%) and high-Cr (Cr_2O_3 = 52–56 wt.%) chromspinel widespread in the Uralian ophiolite dunite and chromitites. The consideration of chromite compositions with different discrimination diagrams showed that the most Sabantuy detrital chromites correspond to mantle peridotites of subduction settings. A minor part of chromspinels can be related to volcanic rocks, probably oceanic or island-arc affinity.

Some of the studied chromspinels rarely contain inclusions that can be classified as solid-state monomineralic, polymineralic and melt inclusions. No platinum-group minerals were found as inclusions within chromite. The monomineralic inclusions are mainly represented by high-magnesian olivine, orthopyroxene, chrome-diopside and amphibole. The composition of these minerals corroborates their genetic affinity to peridotites. The bulk composition of melt inclusions and the composition of preserved glass corresponds to basalts and andesites, indicating the volcanic nature of host chromite.

The whole set of the obtained data indicates that most Sabantuy chromites came from peridotites and chromitites of the Uralian ophiolite complexes, including ophiolite allochthones transferred from the Main Uralian Fault zone westward during the Late Paleozoic collision. The huge Kraka peridotite allochthon comprising numerous small chromite occurrences and several economically important deposits is the closest to the Sabantuy paleoplacer and may represent a suitable provenance source of chromite. Chromites could be also derived from mafic and ultramafic volcanic rocks formed during the oceanic and island-arc stage of the Urals evolution. It is also possible that chromspinel were transferred from ancient Archean and Proterozoic mafic–ultramafic layered intrusions and volcanics, widespread in the western slope of the Urals (Bashkirian Anticlinorium). Our data may indicate that chromspinels could be transported over longer distances than was previously accepted.

Supplementary Materials: The following are available online at https://www.mdpi.com/article/10.3390/min11070691/s1, Table S1: Composition of ore minerals.

Author Contributions: Sampling, investigations, analytical results and interpretation, I.R.R., E.V.P. and I.A.G. Writing the paper, conclusions, I.R.R. and E.V.P. All authors have read and agreed to the published version of the manuscript.

Funding: This research was funded by the Council of the President of the Russian Federation, grant number MK-857.2021.1.5 and State Contract of IG UFRC RAS (no. 0246-2019-0080). The analytical studies were supported by State scientific program AAAA-A18-118052590029-6. The authors are grateful to Scientific Center "Geoanalitik" Institute of Geology and Geochemistry UB RAS, Yekaterinburg, carrying out microprobe and SEM studies.

Data Availability Statement: The data presented in this study are available on request from the corresponding author.

Acknowledgments: The authors are grateful to four anonymous reviewers for comments and recommendations that allow significantly improved our manuscript. We thank Dmitri Saveliev, Sergey Michurin and Andrey Vishnevskiy for their assistance in analytical work. We are grateful to T.A. Miroshnichenko for the English translation of our manuscript.

Conflicts of Interest: The authors declare no conflict of interest.

References

1. Irvine, T.N. Chromium spinel as a petrogenetic indicator. Part, I. Theory. *Can. J. Earth Sci.* **1965**, *2*, 648–672. [CrossRef]
2. Irvine, T.N. Chromium spinel as a petrogenetic indicator. Part II. Petrological applications. *Can. J. Earth Sci.* **1967**, *4*, 71–103. [CrossRef]
3. Dick, H.J.B.; Bullen, T. Chromian spinel as a petrogenetic indicator in abyssal and alpine-type peridotites and spatially associated lavas. *Contrib. Mineral. Petrol.* **1984**, *86*, 54–76. [CrossRef]
4. Arai, S. Characterization of spinel peridotites by olivine-spinel compositional relationships: Review and interpretation. *Chem. Geol.* **1994**, *113*, 191–204. [CrossRef]
5. Sack, R.O.; Ghiorso, M.S. Chromite as a petrogenetic indicator. In *Oxide Minerals: Petrologic and Magnetic Significance*; Lindsley, D.H., Ed.; Mineralogical Society of America: Chantilly, VA, USA, 1991; Volume 25, pp. 323–353.
6. Maslov, A.V.; Mizens, G.A.; Badida, L.V.; Krupenin, M.T.; Vovna, G.M.; Kiselev, V.I.; Ronkin, Y.L. *Lithogeochemistry of Terrigenous Associations of the Southern Depressions of the Ural Foredeep*; IGG UB RAS: Yekaterinburg, Russia, 2015; p. 308. (In Russian)
7. Mizens, G.A.; Maslov, A.V. Sandstones from the molasse formation in the southern part of the Uralian foredeep. *Lithol. Miner. Resour.* **2015**, *50*, 407–431. [CrossRef]
8. Gujar, A.R.; Ambre, N.V.; Iyer, S.D.; Mislankar, P.G.; Loveson, V.J. Placer chromite along south Maharashtra, central west coast of India. *Curr. Sci.* **2010**, *99*, 492–499.
9. Pober, E.; Faupl, P. The chemistry of detrital spinels and its implications for the geodynamic evolution of the eastern Alps. *Geologische Rundschau* **1988**, *77*, 641–670. [CrossRef]
10. Emory-Moore, M.; Scott, W.J.; Davis, L. Detrital chromite concentrations, nearshore Port au Port Bay, Newfoundland. *Atl. Geol.* **1992**, *28*, 233–241.
11. Hisada, K.; Arai, S. Detrital chrome spinels in the cretaceous sanchu sandstone, central Japan: Indicator of serpentinite protrusion into a fore-arc region. *Palaeogeogr. Palaeoclim. Palaeoecol.* **1993**, *105*, 95–109. [CrossRef]
12. Hisada, K.I.; Arai, S.; Lee, Y.I. Tectonic implication of lower cretaceous chromian spinel-bearing sandstones in Japan and Korea. *Isl. Arc* **1999**, *8*, 336–348. [CrossRef]
13. Lenaz, D.; Kamenetsky, V.S.; Crowford, A.J.; Princivalle, F. Melt inclusions in detrital spinel from the SE Alps (Italy–Slovenia): A new approach to provenance studies of sedimentary basins. *Contrib. Mineral. Petrol.* **2000**, *139*, 748–758. [CrossRef]
14. Oberhänsli, R.; Wendt, A.S.; Goffé, B.; Michard, A. Detrital chromites in metasediments of the east-Arabian continental margin in the Saih Hatat area: Constraints for the palaeogeographic setting of the Hawasina and Semail basins (Oman mountains). *Int. J. Earth Sci.* **1999**, *88*, 13–25. [CrossRef]
15. Zhu, B.; Kidd, W.S.F.; Rowley, D.B.; Currie, B.S. Chemical compositions and tectonic significance of chrome-rich spinels in the Tianba Flysch, southern Tibet. *J. Geol.* **2004**, *112*, 417–434. [CrossRef]
16. Faupl, P.; Pavlopoulos, A.; Klötzli, U.; Petrakakis, K. On the provenance of mid-cretaceous turbidites of the Pindos zone (Greece): Implications from heavy mineral distribution, detrital zircon ages and chrome spinel chemistry. *Geol. Mag.* **2006**, *143*, 329–342. [CrossRef]
17. Pownceby, M.; Bourne, P. Detrital chrome-spinel grains in heavy-mineral sand deposits from southeast Africa. *Mineral. Mag.* **2006**, *70*, 51–64. [CrossRef]
18. Al-Juboury, A.I.; Ghazal, M.M.; Mccann, T. Detrital chromian spinels from miocene and holocene sediments of northern Iraq: Provenance implications. *J. Geosci.* **2009**, *54*, 289–300. [CrossRef]
19. Pirnia, T.; Arai, S.; Torabi, G. A Better picture of the mantle section of the Nain ophiolite inferred from detrital chromian spinels. *J. Geol.* **2013**, *121*, 645–661. [CrossRef]
20. Baxter, A.T.; Aitchison, J.C.; Ali, J.R.; Chan, J.S.-L.; Chan, G.H.N. Detrital chrome spinel evidence for a neotethyan intra-oceanic island arc collision with India in the paleocene. *J. Asian Earth Sci.* **2016**, *128*, 90–104. [CrossRef]
21. Bónová, K.; Mikuš, T.; Bóna, J. Is Cr-spinel geochemistry enough for solving the provenance dilemma? Case study from the Palaeogene sandstones of the western Carpathians (eastern Slovakia). *Minerals* **2018**, *8*, 543. [CrossRef]
22. Puchkov, V.N. *Paleogeodynamics of the Southern and Middle Urals*; Gilem: Ufa, Russia, 2000; p. 146. (In Russian)
23. Brown, D.; Herrington, R.J.; Alvarez-Marron, J. Processes of arc–continent collision in the uralides. In *Arc-Continent Collision Frontiers in Earth Sciences*; Brown, D., Ryan, P.D., Eds.; Springer: Berlin/Heidelberg, Germany, 2011; pp. 311–340.
24. Puchkov, V.N. Structural stages and evolution of the Urals. *Mineral. Petrol.* **2013**, *107*, 3–37. [CrossRef]
25. Abdulmazitov, H.D.; Baymukhametov, K.S.; Victorin, V.D. *Geology and Development of the Largest and Unique Oil and Gas-Oil Fields in Russia*, 2nd ed.; Gavura, V.E., Ed.; VNIIOENG: Moscow, Russia, 1996; Volume 1, p. 280. (In Russian)
26. Kudryashov, A.I. *Verkhnekamskoe Salt Deposit*; MI UB RAS: Perm, Russia, 2001; p. 429. (In Russian)
27. Volkov, A.V.; Novikov, I.A.; Razumovsky, A.A.; Murashov, K.Y.; Sidorova, N.V. Geochemical features and formation conditions of the cupriferous sandstones of the Orenburg pre-Urals. *Lithosphere* **2018**, *4*, 593–606. (In Russian) [CrossRef]
28. Alekseev, A.A.; Alekseeva, G.V.; Kovalev, S.G. *Layered Intrusions of the Western Slope of the Urals*; Gilem: Ufa, Russia, 2000; p. 188. (In Russian)
29. Savelieva, G.N. *Gabbro-Ultrabasite Assemblages of the Urals Ophiolites and Their Analogues in Modern Oceanic Crust*; Transactions of the Geological Institute, Academy of Science 404; Nauka: Moscow, Russia, 1987; p. 242. (In Russian)
30. Savelieva, G.N.; Nesbitt, R.Q. A Synthesis of the stratigraphic and tectonic setting of the Uralian ophiolites. *J. Geol. Soc.* **1996**, *153*, 525–537. [CrossRef]

31. Savelieva, G.N.; Sharaskin, A.Y.; Saveliev, A.A.; Spadea, P.; Pertsev, A.N.; Babarina, I.I. Ophiolites and zoned mafic-ultramafic massifs of the Urals: A comparative analysis and some tectonic implications. In *Mountain building in the Uralides: Pangea to Present*; Brown, D., Juhlin, C., Puchkov, V., Eds.; AGU Monograph: Washington, DC, USA, 2002; pp. 135–153.
32. Krause, J.; Brügmann, G.E.; Pushkarev, E.V. Accessory and rock forming minerals monitoring the evolution of zoned mafic-ultramafic complexes in the central Ural mountains. *Lithos* **2007**, *95*, 19–42. [CrossRef]
33. Krause, J.; Brügmann, G.E.; Pushkarev, E.V. Chemical composition of spinel from Uralian-Alaskan-type mafic–ultramafic complexes and its petrogenetic significance. *Contrib. Mineral. Petrol.* **2011**, *161*, 255–273. [CrossRef]
34. Garuti, G.; Pushkarev, E.V.; Thalhammer, O.A.R.; Zaccarini, F. Chromitites of the Urals (part 1): Overview of chromite mineral chemistry and geotectonic setting. *Ofioliti* **2012**, *37*, 27–53.
35. Perevozchikov, B.V. (Ed.) *The Registry of Chromite Deposits in Alpine-Type Ultramafites of the Urals*; KamaRICSDI: Perm, Russia, 2000; p. 474. (In Russian)
36. Patyk-Kara, N.G.; Zubkov, L.B.; Bykhovsky, L.Z.; Ryzhov, B.V.; Benevolsky, B.I. *Placer Deposits of Russia and Other Countries of Union of Independent States*; Scientific World: Moscow, Russia, 1995; p. 454.
37. Rakhimov, I.R.; Saveliev, D.E.; Kholodnov, V.V.; Zamyatin, D.A. The unique sabantuy chromite paleoplacer in the sedimentary cover of the eastern European platform. *Geol. Ore Depos.* **2020**, *62*, 542–546. [CrossRef]
38. Knyazev, Y.G.; Knyazeva, O.Y.; Snachev, V.I.; Zhdanov, A.V.; Karimov, T.R.; Aydarov, E.M.; Masagutov, R.K.; Arslanova, E.R. *State Geological Map of the Russian Federation*, 3rd ed.; Scale 1:1,000,000; Ural series. N-40-Ufa; Explanatory Letter; VSEGEI: St. Petersburg, Russia, 2013; p. 512. (In Russian)
39. Lucas, S.G.; Shen, S.-Z. The Permian chronostratigraphic scale: History, status and prospectus. In *The Permian Timescale*; Special Publications; Lucas, S.G., Shen, S.Z., Eds.; Geological Society: London, UK, 2018; Volume 450, pp. 21–50.
40. Russell, R.D.; Taylor, R.E. Roundness and shape of Mississippi river sands. *J. Geol.* **1937**, *45*, 225–267. [CrossRef]
41. Pettijohn, F.J.; Potter, P.E.; Siever, R. *Sand and Sandstone*, 2nd ed.; Springer: New York, NY, USA, 1987; p. 560.
42. Barnes, S.J.; Roeder, P.I. The range of spinel compositions in terrestrial mafic and ultramafic rocks. *J. Petrol.* **2001**, *42*, 2279–2302. [CrossRef]
43. Ishii, T.; Robinson, P.T.; Maekawa, H.; Fiske, M. Petrological studies from diapiric serpentine seamounts in the Izu–Ogazawara–Mariana forearc. In *Proceedings of the Ocean Drilling Program*; Scientific Results; Fryer, P., Pearce, J.A., Stokking, L.B., Eds.; Texas A&M University: College Station, TX, USA, 1992; Volume 125, pp. 445–485.
44. Evans, B.W.; Frost, B.R. Chrome-spine1 in progressive metamorphism: A preliminary analysis. *Geochim. Cosmochim. Acta* **1975**, *39*, 959–972. [CrossRef]
45. Kamenetsky, V.S.; Crawford, A.J.; Meffre, S. Factors controlling chemistry of magmatic spinel: An empirical study of associated olivine, Cr-spinel and melt inclusions from primitive rocks. *J. Petrol.* **2001**, *42*, 655–671. [CrossRef]
46. Saveliev, D.E. Chromitites of the kraka ophiolite (south Urals, Russia): Geological, mineralogical and structural features. *Miner. Depos.* **2021**. [CrossRef]
47. Lehmann, J. Diffusion between olivine and spinel: Application to geothermometry. *Earth Planet. Sci. Lett.* **1983**, *64*, 123–138. [CrossRef]
48. Arai, S. Chemistry of chromian spinel in volcanic rocks as a potential guide to magma chemistry. *Miner. Mag.* **1992**, *56*, 173–184. [CrossRef]
49. Gilbert, M.C.; Helz, R.T.; Popp, R.K.; Spear, F.S. Experimental studies of amphibole stability. In *Amphiboles: Petrology and Experimental Phase Relations*; Veblen, D.R., Ribbe, P.H., Eds.; De Gruyter: Berlin, Germany, 1982; Volume 9, pp. 229–253.
50. Mizens, G.A. *Upper Paleozoic Flysch of the Western Urals*; Ural Branch of the Russian Academy of Sciences: Ekaterinburg, Russia, 1997; p. 230. (In Russian)
51. Afanasyev, V.P.; Pokhilenko, N.P.; Logvinova, A.M.; Zinchuk, N.N.; Efimova, E.S.; Krasavchikov, V.O.; Podgornykh, N.M.; Prugov, V.P. New morphogenetic type of Cr-spinellide in diamondiferous areas in connection with the problem of false kimberlite indicators. *Rus. Geol. Geophys.* **2000**, *41*, 1729–1741. (In Russian)
52. Bhatta, K.; Ghosh, B. Chromian spinel-rich black sands from eastern shoreline of Andaman island, India: Implication for source characteristics. *J. Earth Syst. Sci.* **2014**, *123*, 1387–1397. [CrossRef]
53. Berzin, S.V. Ophiolites of the Mariinsky complex at east and west frames of the Revdinsky Massif. *Lithosphere* **2016**, *1*, 88–106. (In Russian)
54. Kosarev, A.M.; Svetov, S.A.; Chazhengina, S.Y.; Shafigullina, G.T. Boninitic variolites of the Buribay volcanic complex in the southern Urals: Mineralogy, geochemistry and formation conditions. *Lithosphere* **2018**, *18*, 246–279. (In Russian) [CrossRef]
55. Pushkarev, E.V.; Ryazantsev, A.V.; Gottman, I.A. Ankaramites of the Prisakmar-Voznesenska zone in the southern Urals—Geological settings and composition. In *Year-Book-2016*; Institute of Geology and Geochemistry UB RAS: Yekaterinburg, Russia, 2017; Volume 164, pp. 166–175. (In Russian)
56. Pushkarev, E.V.; Ryazantsev, A.V.; Gottman, I.A.; Degtyarev, K.E.; Kamenetsky, V.S. Ankaramite: A new type of high-magnesium and high-calcium primitive melt in the Magnitogorsk island-arc zone (southern Urals). *Doklady Earth Sci.* **2018**, *479*, 463–467. [CrossRef]
57. Shilo, N.A. *Teaching on Placer Deposits*; Dalnauka: Vladivostok, Russia, 2002; p. 576. ISBN 5-8044-0200-5. (In Russian)
58. Roeder, P.l.; Poustovetov, A.; Oskarsson, N. Growth forms and composition of chromian spinel in MORB magma: Diffusion-controlled crystallization of chromian spinel. *Can. Mineral.* **2001**, *39*, 397–416. [CrossRef]

59. Sack, R.O.; Ghiorso, M.S. Chromian spinels as petrogenetic indicators: Thermodynamics and petrological applications. *Am. Miner.* **1991**, *76*, 827–847.
60. Paneyakh, N.A. Evolutuion of the spinel compositions in ultramafites. *Miner. J.* **1984**, *6*, 38–52.
61. Chaschukhin, I.S.; Votyakov, S.L.; Shapova, Y.V. *Crystallochemistry of Chromspinel and Oxythermobarometry of Ultramafites of Folded Belts*; Koroteev, V.A., Ed.; Institute of Geology and Geochemistry Ural Branch RAS: Yekaterinburg, Russia, 2007; p. 310. (In Russian)
62. Ghosh, B.; Morishita, T.; Bhatta, K. Significance of chromian spinels from the mantle sequence of the andaman ophiolite, India: Paleogeodynamic implications. *Lithos* **2013**, *164*, 86–96. [CrossRef]